

## Journal Pre-proof

Photocatalysis of Dyes: Operational Parameters, Mechanisms, and Degradation Pathway

Shi Nin Tan , Mei Lian Yuen , Ros Azlinawati Ramli

PII: S2772-5774(25)00027-8  
DOI: <https://doi.org/10.1016/j.greeac.2025.100230>  
Reference: GREEAC 100230



To appear in: *Green Analytical Chemistry*

Received date: 26 December 2024  
Revised date: 18 February 2025  
Accepted date: 20 February 2025

Please cite this article as: Shi Nin Tan , Mei Lian Yuen , Ros Azlinawati Ramli , Photocatalysis of Dyes: Operational Parameters, Mechanisms, and Degradation Pathway, *Green Analytical Chemistry* (2025), doi: <https://doi.org/10.1016/j.greeac.2025.100230>

This is a PDF file of an article that has undergone enhancements after acceptance, such as the addition of a cover page and metadata, and formatting for readability, but it is not yet the definitive version of record. This version will undergo additional copyediting, typesetting and review before it is published in its final form, but we are providing this version to give early visibility of the article. Please note that, during the production process, errors may be discovered which could affect the content, and all legal disclaimers that apply to the journal pertain.

© 2025 Published by Elsevier B.V.

This is an open access article under the CC BY-NC-ND license (<http://creativecommons.org/licenses/by-nc-nd/4.0/>)

## HIGHLIGHTS

- Effect of various parameters during the photocatalysis process.
- Mechanism of photocatalysis involvement of oxidising and reducing agents.
- Analytical techniques for determining intermediates of MB and RhB.
- Photocatalysis steps: Demethylation, ring shortening, ring-opening, and mineralisation.
- Postulated degradation pathway of MB and RhB.

Journal Pre-proof

# Photocatalysis of Dyes: Operational Parameters, Mechanisms, and Degradation Pathway

Shi Nin Tan, Mei Lian Yuen\*, Ros Azlinawati Ramli

Faculty of Industrial Sciences and Technology, Universiti Malaysia Pahang Al-Sultan

Abdullah, Lebu Persiaran Tun Khalil Yaakob, 26300 Kuantan, Pahang, Malaysia.

[tanshinin98@gmail.com](mailto:tanshinin98@gmail.com), [yuenm@umpsa.edu.my](mailto:yuenm@umpsa.edu.my)\*, [azlinawati@umpsa.edu.my](mailto:azlinawati@umpsa.edu.my)

\* Corresponding author

Email Address: [yuenm@umpsa.edu.my](mailto:yuenm@umpsa.edu.my) (Mei Lian Yuen)

## ABSTRACT

Photocatalysis is an advanced oxidation process (AOP) that has significant attention to the degradation of organic pollutants. Although most literature on photocatalysis mainly focuses on the basic photocatalytic mechanisms, photocatalyst designs, and operational parameters, this research aims to delve deeply into the various process parameters and mechanisms under different conditions. It explores intermediates produced by dye photocatalysis and the proposed degradation pathways. This review systematically analysed relevant literature based on various databases, studying various process parameters and mechanisms as well as utilising analytical techniques (spectroscopy and chromatography) to synthesise key themes and findings in photocatalysis. This review revealed significant advancements in photocatalysis, highlighting the photocatalytic process has 4 domain steps in degradation pathways, including demethylation, ring shortening, ring opening, and mineralisation. Previous studies indicated the emergence of new peaks at 331 nm and 370 nm in UV-Vis analysis for MB, while hypsochromic shifts for RhB were attributed to the processes of demethylation and de-ethylation, respectively. In short, this review underscores the potential of dye photocatalysis to revolutionise green analytical practices and emphasises the importance of sustainable approaches in analytical methodologies, focusing on innovative and eco-friendly analytical methods aligned with the scope of the journal.

**Keywords:** Photocatalysis, photocatalytic mechanisms, degradation pathway, analytical techniques, intermediates.

## 1. Introduction

As the fast fashion trend develops, the demand for new clothing increases year by year, leading to increased production and environmental concerns. The production of new clothing has required essential resources such as water and energy. A massive amount of water, approximately 1.6 million litres of water has been consumed by the textile industry for the production of 8 tonnes of fabrics [1]. Also, water used by the textile industry is released into the environment along with approximately 72 toxic chemicals [2]. Among these chemicals, synthetic dyes are a significant concern due to their toxicity and hazard to the environment and human health.

In order to treat the dye wastewater before it returns to water bodies, there are some methods, such as physical, biological, and chemical, that have been studied by researchers. Physical approaches such as adsorption treatment, membrane filtration, and coagulation can achieve a high dye removal from wastewater [3–5]. Elzahar & Bassyouni [6] reported that chitosan as an adsorbent achieved up to 94.2% removal of Direct Blue 78. Moreover, activated carbon is also a prevalent adsorbent in dye wastewater treatment, as it can achieve a 99.5% removal percentage of Reactive Red 195 [7]. However, there are drawbacks to these physical approaches, such as high cost, post-treatment of adsorbents and sludge, and membrane fouling [8–11]. On the other hand, biological approaches include the bioremediation of dye by the facilitation of fungi, bacteria, algae, and enzymes. Takkar et al. [12] reported that *Actinobacillus* biodegradation of methyl red demonstrated a high removal percentage of 98.9% within 12 hours. Besides, Sonwani et al. [13] revealed that the removal percentage of Congo red (CR) reached up to 97.0% using an anaerobic-aerobic sequential bioreactor. This process took up to 12 days to complete the decolorisation. Although biological approaches have been used to remove dyes from wastewater completely, the process is prolonged and essential for managing critical conditions that demand meticulous monitoring.

Chemical methods, also known as advanced oxidation processes (AOPs), utilise chemicals such as oxidative reagents to generate reactive oxygen species (ROS) to treat dye wastewater. Researchers have extensively studied dye wastewater treatment by photocatalytic degradation [14–16]. This is because photocatalytic degradation essentially degrades and mineralises dye molecules by introducing natural resources into the process, forming fewer or no harmful products. Furthermore, the excellent performance of semiconductor photocatalysts such as  $\text{TiO}_2$ ,  $\text{ZnO}$ ,  $\text{Bi}_2\text{O}_3$ , rGO, and carbon dots in dye

degradation and the recyclability of heterogeneous photocatalysts are the plus points of this process [17–20]. For example, Bilici et al. [21] demonstrated that  $\text{TiO}_2$  as the heterogeneous semiconductor photocatalyst with the amount of 1.0 g/L achieved complete photodegradation of 50 ppm of Reactive Orange in the presence of hydrogen peroxide ( $\text{H}_2\text{O}_2$ ). After five consecutive cycles of reuse, the photodegradation efficiency remained steady. This demonstrates the sustainability and longevity of semiconductors as photocatalysts.

The photodegradation process promotes sustainable solutions for monitoring and controlling dye pollutants in the environment. Utilising natural resources such as sunlight or low-energy light in the photocatalytic process helps minimise waste generation in industry while reducing energy consumption. Furthermore, the photocatalysts used in the literature are mostly sustainable and multifunctional, which in turn contributes to green chemistry principles. Further developments in dye photocatalysis, including the use of sustainable materials such as agricultural waste and natural resources, will significantly drive innovation in environmentally friendly analytical methods.

It is gratifying to ascertain that the photodegradation of dye wastewater is highly dependent on environmental effects. By meticulously examining various operation effects, researchers can evaluate the operating conditions to achieve a maximum photodegradation percentage, allowing for the implementation of this approach on an industrial scale in the future. Therefore, the purpose of this review is to summarise the effects of environmental variables, including light source and intensity, photocatalyst dosage, initial pH and initial concentration of the dye solution, reaction temperature, and the presence of oxidising and reducing agents, on the performance of photocatalysts for dye degradation. In addition, in order to gain an in-depth understanding of photocatalytic degradation, its mechanism will be encapsulated, thereby providing bonus points for optimising the conditions for the photocatalytic degradation process. There is a paucity of information on exploring the intermediates by various analytical instruments in the previous review articles. In light of this, this review presented herein aims to outline the technique of analysing intermediates produced during the photocatalytic degradation of azo and xanthene dyes.

## 2. Parameter effects on photodegradation

Photodegradation efficiency is a critical determinant of photocatalyst longevity and availability. Nonetheless, the efficiency of photocatalysts is highly dependent on various process parameters. Operational parameters such as light source and intensity, photocatalyst dosage, initial pH of the solution, initial dye concentration, reaction temperature, oxidising agent, and reducing agent are particularly important due to their substantial impact on dye degradation performance.

### 2.1 Effects on light source and intensity

Photodegradation, as the name implies, is the process of breaking down substances in the presence of light. Hence, light plays a vital role in the photocatalysis process. Due to the adsorption of light by dyes and photocatalysts at different wavelengths, the type of illumination chosen becomes a crucial consideration. Types of light can be divided into three categories: (i) ultraviolet (100-400 nm), (ii) visible (400-700 nm), and (iii) near-infrared (700-1000 nm). In the field of photocatalytic degradation, sunlight, ultraviolet (UV) light, and visible light are widely studied because semiconductor photocatalysts are more sensitive to the absorption wavelengths of these light sources. UV light can be categorised into three types: UVA (315-400 nm), UVB (280-315 nm), and UVC (100-280 nm) [22].

Wang et al. [23] found that 20 mg/L reactive red was substantially degraded under UV light at wavelengths 185 and 254 nm in the presence of sodium persulphate ( $\text{Na}_2\text{S}_2\text{O}_8$ ). Ozone ( $\text{O}_3$ ) is favourable to generate hydroxyl radicals ( $\bullet\text{OH}$ ) by direct photolysis under UV light with a wavelength of 185 nm, while persulphate ions ( $\text{S}_2\text{O}_8^-$ ) are favourably activated to form sulphate radicals ( $\text{SO}_4^-$ ) at the wavelength of 254 nm. In addition, an effort has been made by Ayodhya et al. [24] to compare the different light sources (sunlight, visible, and UV) to photodegrade various organic dyes by copper sulphide (CuS) nanoparticles for 4 hours of irradiation times. They demonstrate that the photodegradation of organic dyes under sunlight irradiation reached the highest removal percentage. Likewise, according to Safni et al. [25], when evaluating the effectiveness of CN-codoped  $\text{TiO}_2$  in photodegrading orange F3R dye under various light, the order of photodegradation ability from lowest to highest is as follows: visible light, UV light, and sunlight. The photodegradation efficiency of 6 mg of CN co-doped  $\text{TiO}_2$  on 30 mg/L orange F3R dye under sunlight reached 53.9%. This is because of the wide range of wavelengths in the sunlight spectrum, which allows it to effectively photodegrade dyes. By contrast, UV and

visible lights showed moderate effectiveness in degrading dyes, around 30%. Therefore, it is preferential to undergo photocatalytic degradation of dyes under sunlight irradiation.

Besides light sources, light intensity is also a key point in the photodegradation of dyes. This is because light intensity affects the dye photodegradation kinetics, as mentioned by Groeneveld et al. [26] and Ollis [27] in Table 1.

Table 1: The relationship between photodegradation rate and light intensity [26, 27].

Light intensity	Description
Low (0-20 mW/cm <sup>2</sup> )	A linear relationship between photodegradation rate and light intensity First kinetic order ( $Rate = k[I]$ )
Intermediate (25 mW/cm <sup>2</sup> )	The photodegradation rate is dependent on the square root of light intensity Half kinetic order ( $Rate = k[I]^{\frac{1}{2}}$ )
High (>25 mW/cm <sup>2</sup> )	The photodegradation rate is independent of light intensity Zero kinetic order ( $Rate = k[I]^0$ )

Moreover, as the light intensity increases, the photon number increases, thus enhancing the generation of ROS. As reported by Ilyas et al. [28], the degradation efficiency of 15 mg/L of crystal violet (CV) at 60 min was positively correlated with light intensity, where the visible light intensity increased from  $20 \times 10^3$  Lux to  $55 \times 10^3$  Lux, resulting in an increase in the degradation percentage from 42.1% to 100%. Furthermore, Zhang et al. [29] highlighted partially different trends in photodegradation efficiency with increasing light intensity. With the systematic increase of UV light intensity (200-400 W), the photodegradation of 50 mg/L of Rhodamine B (RhB) by 40 mg of Bi<sub>2</sub>O<sub>3</sub>@LDHs within 180 min showed a noticeable trend from 50.0% to 90.4%, followed by only 5% variation increment in degradation efficiency after reaching 400 W. Thus, a further increase in light intensity no longer resulted in significant changes. This trend highlights the photodegradation rate of dye is independent of light intensity when reaching a threshold value. Similarly, as the intensity increased from 60 lux to 70 lux, the efficiency of TiO<sub>2</sub>/GO nanocomposite in photodegrading Malachite Green (MG) under a Xenon lamp increased from approximately 69% to 82% and subsequently decreased to 76% (75 lux) [30].

From these findings, the type of light source and light intensity significantly influenced the degradation efficiency of the dye. Sunlight, as a sustainable energy source, is crucial for exploring photocatalysis. Moreover, it is essential to identify the optimal level of light

intensity to achieve a maximum photodegradation rate without escalation of cost. Therefore, these hierarchies emphasise the significance of determining the appropriate irradiation wavelength and light intensity in accordance with the particular requirements of photocatalytic degradation.

## 2.2 Effects on photocatalyst dosage

In order to achieve a maximum dye degradation percentage, the researchers conducted studies to determine the effect of photocatalyst dosage on the degradation of dye. Generally, when the amount of photocatalyst increases, the decolorisation percentage increases significantly [31]. This is attributed to the increased surface area, thus providing more available active sites for the adsorption of dye [32]. Ariyanti et al. [33] proved that the photodegradation efficiency of 5 ppm RhB and methyl orange (MO) in single and binary systems increased with the increase of photocatalyst (0.5-2.0 g/L). Furthermore, a similar consequence was shown in the work of Ahmadi & Ganjidoost [34], in which zinc oxide immobilised banana peel activated carbon (BPAC/ZnO) nanocomposite was employed as a photocatalyst for photodegradation of Acid Blue 25 (AB25). The nanocomposite dosage has increased from 0.2 g to 0.9 g, which enhanced the degradation of AB25 from 77% to 97%. In addition, Bagheri & Chaibakhsh [35] reported that the photocatalytic ozonation of Acid Blue 113 (AB113) by Fe<sub>2</sub>O<sub>2</sub>/MoS<sub>2</sub>, resulted in an upward trend in photodegradation efficiency with the increased photocatalyst dosage (1-15 mg). An outstanding degradation performance occurred when Fe<sub>2</sub>O<sub>2</sub>/MoS<sub>2</sub> was increased to 15 mg, providing a complete decolorisation of AB113. Herein, increasing photocatalyst dosage leads to the escalation of available active sites, enhancing the adsorption of O<sub>3</sub>, and thereby generating more ROS, which may contribute to the subsequent oxidation of organic pollutants.

However, when photocatalyst loading is surplus, the degradation performance of the dye is reduced. This limits mass transfer and UV scattering, thereby reducing dye removal efficiency [36, 37]. As reported by Bhapkar et al. [38], whose work demonstrated that the photodegradation of 5 ppm methylene blue (MB) by ZnO was enhanced when the photocatalyst dosage increased from 0.05 g/L to 0.1 g/L. However, when the ZnO dosage increased to 0.15 g/L, the degradation efficiency decreased slightly from 97.21% to 94.46%. A similar outcome was reported by Ilyas et al. [28]. In photocatalytic degradation of 15 mg/L CV, a markedly increased degradation efficiency from 48.54% to 99.12% as the amount of Au@Vm-BiVO<sub>4</sub> increased from 5 mg to 25 mg. As the dosage of Au@Vm-BiVO<sub>4</sub> further increased (30 mg), the degradation efficiency decreased (92.92%).



Essentially, photocatalysts, as photocatalytic accelerators, play a key role in affecting dye degradation efficiency. The photodegradation efficiency increases with the increment of photocatalyst amount and subsequently declines after reaching the threshold. This indicates that an appropriate dosage of photocatalyst is imperative to achieve optimal photodegradation efficiency.

### *2.3 Effects on initial pH of solution*

In the photocatalytic process, the initial pH of the dye solution has a great influence on the adsorption dynamics and the generation of ROS, thereby affecting the degradation efficiency of the dye [39, 40]. The point of zero charge (PZC) is the basic concept for studying the effect of the initial pH value of a dye solution on the photodegradation of dyes. In general, when the initial pH value of the dye solution is lower than the  $\text{pH}_{(\text{PZC})}$  value, the photocatalyst is presumed to have a positively charged surface. In contrast, when the pH of the solution is higher than  $\text{pH}_{(\text{PZC})}$ , the photocatalyst surface provides negative charges [41]. When the surface of the photocatalyst is positively charged, it is conducive to the adsorption of anionic dyes through electrostatic attraction [42]. Conversely, the negatively charged photocatalyst surface is more favourable for the adsorption of cationic dyes.

Recent studies have shown that the  $\text{pH}_{(\text{PZC})}$  significantly impacts the photocatalytic efficiency of photocatalysts, confirming the importance of charge interactions in promoting dye adsorption. For instance, Bhapkar et al. [38] reported that the initial pH value of the 5 ppm MB solution was 4, which was lower than the  $\text{pH}_{(\text{PZC})}$  of ZnO (pH 7.6), resulting in a low degradation performance (27%). This is attributed to the positive charge on the ZnO surface, resulting in Coulomb repulsion between the dye and the photocatalyst. Therefore, the adsorption of MB dye on the ZnO was weak. On the other hand, when the initial pH of MB was 9, the ZnO surface favoured the cationic properties of MB through electrostatic attraction, which resulted in a photodegradation efficiency of 98%. According to studies by Yusuff et al. [43], zinc oxide-termite hill composite (ZnO-TH) had a  $\text{pH}_{(\text{PZC})}$  of 7.72 and decolorised 25 mg/L AB113 by about 92.3% at pH 3 and less than 60% at pH 10. At the low pH of the solution, the positively charged surface of ZnO-TH was conducive to the adsorption of the AB113 of anionic dye by electrostatic attraction, thereby increasing the interaction between the dye and the generated ROS on the surface of the photocatalyst. Conversely, the negatively charged surface of ZnO-TH at a high pH value hindered the adsorption of AB113 dye by repulsive force, resulting in decreased photodegradation efficiency.

The initial pH of the solution also significantly influences the generation of ROS in the photocatalysis process, especially in the photocatalytic ozonation.  $O_3$  is an oxidant that is favourable to acidic conditions, as  $O_3$  undergoes two possible mechanisms: (i) direct oxidation and (ii) indirect oxidation. In direct oxidation,  $O_3$  destroys the carbon double bonds (C=C) of the aromatic rings to produce intermediates of aldehydes and carboxylic acid [44, 45]. Meanwhile, indirect oxidation is highly dependent on the pH value of the reactant solution. Under acidic conditions, the environment of the reactants consists of a high concentration of hydrogen ions ( $H^+$ ), which enhances the electrophilic attack of organic dye. By contrast, there is an adverse effect on dye photodegradation when  $O_3$  is under an alkaline condition [46]. In previous studies, the photocatalytic ozonation of 50 ppm Direct Blue 1 (DB1) by 7.5 mg of  $ZnSnO_3@S$ -doped  $g-C_3N_4$  attained the most promising results at pH 2 (~45%), mild photodegradation efficiency at pH 3 and pH 5 (~30% and ~20%, respectively), and lower photodegradation efficiencies after pH 5 (less than 20%) across a wide range of pH values (pH 2-12) [47]. However, to imitate the real scenario in textile wastewater, a weak acidic condition of reactant solution is selected instead of a strong acidic condition.

The photo-Fenton process has different effects on pH compared to photocatalytic degradation and photocatalytic ozonation processes. Chakraborty et al. [48] reported that the degradation efficiency of 50 ppm MB and CR decreased with increasing pH. While at pH 2, MB and CR were almost completely degraded. This is because the surface of ferrous nanoparticles becomes more positively charged, which enhances dye adsorption, consequently promoting the capacity for degradation. Whereas, under alkaline conditions, the high concentration of  $OH^-$  ions reacts with Fe nanoparticles to form ferric hydroxide ( $Fe(OH)_3$ ), resulting in a dye removal percentage of less than 50%. Contrary to the former findings, Butt et al. [49] found slightly different results, indicating that complete decolorisation of 10 mg/L MO by 1000 mg/L of ilmenite was in the pH 2-3 but had a slower degradation rate at pH 2 compared to pH 2.5 and 3. This minor discrepancy may be attributable to excessive proton generation, resulting in enhanced  $\bullet OH$  radical scavenging effects [36].

Based on these findings, in different photocatalysis processes, different initial pH levels of solutions are required to achieve optimal degradation effectiveness. The effectiveness of dye degradation highly depends on the adsorption dynamic between dye and photocatalyst. In contrast, photocatalytic ozonation and photo-Fenton are influenced by the interaction of

O<sub>3</sub> molecules and ferrous ions with the concentration of ions (H<sup>+</sup> and OH<sup>-</sup>) present in the solution, thus affecting the generation of ROS.

#### 2.4 Effects on initial dye concentration

At a constant amount of photocatalyst, it is crucial to study the initial dye concentration to determine the optimal conditions for achieving maximum dye removal. Generally, the initial dye concentration is inversely proportional to the effectiveness of degradation of dyes. The decolorisation percentage is projected to decline with the incline of initial dye concentrations. This can be stemmed from the lower capability of photons to penetrate the dye molecules and reach the surface of the photocatalyst [50, 51]. Since dye molecules have occupied the active sites of the photocatalyst, the generation of •OH radicals is reduced, thereby reducing the photodegradation effect of the photocatalyst [52, 53]. Moreover, the high concentration of dye molecules tends to adsorb light, thereby reducing the absorption of light by the photocatalyst surface [54, 55].

A notable example of the effect of initial dye concentrations on photodegradation efficiency is the decreasing trend in the degradation of MB by ZnO as the model contamination concentration increases from 5 ppm (97%) to 15 ppm (84.12%) [38]. Likewise, as noted by Venkatesh et al. [56], photocatalytic degradation of RhB and malachite green oxalate (MGO) by 75 mg of nano SnO<sub>2</sub> demonstrated a significant reduction in degradation efficiency, from 86% to 39% and 94% to 48% for RhB ( $4.35 \times 10^{-6}$  M to  $8.69 \times 10^{-6}$  M) and MGO ( $5.4 \times 10^{-6}$  M to  $2.14 \times 10^{-5}$  M), respectively.

Furthermore, an increase in dye concentration results in an elevation in the number of dye molecules. When the number of dye molecules surpasses the number of •OH radicals produced by O<sub>3</sub> oxidation, the •OH radicals produced are inadequate to degrade the dye molecules. This is certainly true in the case of photocatalytic oxidation of Acid Red 1 (AR 1) with 0.3 g/L TiO<sub>2</sub> and 20% Fe-Zeolite [57]. The increment of AR 1 concentration from 100 ppm to 400 ppm, resulted in decreasing degradation efficiency from approximately 92% to 87%. In addition, as reported by Bousalah et al. [58], the photo-Fenton process with 1.3 mM H<sub>2</sub>O<sub>2</sub> and 0.125 mM of Fe<sup>2+</sup> completely degraded Indigotine in the concentration range of 100-600 ppm under a 100 W tungsten lamp. Nevertheless, the degradation percentage decreased with the rising dye concentrations as the consequence of the high amount of dye molecules hindered the interaction between Fe<sup>2+</sup> ions and H<sub>2</sub>O<sub>2</sub> [59].

However, there are diverging findings from Elsayed et al. [60] and Sharifian et al. [61] with the former. As stated by Elsayed et al. [60], the photodegradation efficiency mainly increased from 90% to approximately 100% as the MB concentration rose from 10 ppm to 50 ppm but then decreased to around 70% when the MB concentration further increased to 100 ppm in the presence of 0.5 g/L of  $\text{WO}_3$  under visible light irradiation for 90 min. Sharifian et al. [61] reported that the removal percentage of MB by 0.8 g/L of  $\text{Ag}@\text{SrTiO}_3 @ \text{CNT}$  nanocomposite was initially increased from 75% to 100% as the dye concentration increased from 2 to 5 ppm, respectively. It can be observed that this occurs only at absolutely low dye concentrations. This may be due to the enhanced interaction between dye molecules and photocatalysts, as well as the lower amount of dye molecules than that of the active site of photocatalysts [62]. Further increased the MB concentration (10 and 20 ppm), the finding ultimately aligned with the formers' findings, in which the photodegradation efficiency dropped to 63% and 54%, respectively.

Accordingly, dye concentration plays a crucial role in the photodegradation process as a reaction rate-related parameter, and it can serve as a pollutant model to simulate real wastewater scenarios. Based on the aforementioned evidence, the maximum photodegradation efficiency was achieved at a lower initial dye concentration. In spite of the fact that low dye concentration can reach a higher removal rate, an appropriate concentration of dye needs to be considered for simulating real wastewater scenarios.

### *2.5 Effects on reaction temperature*

Photodegradation is not a temperature-dependent process, but its kinetic reaction is affected by temperature [63]. Temperature significantly affects the mass transfer of electrons from the valence state to the conduction band as well as the generation of ROS [64]. As the temperature increases, collisions occur between molecules, thereby enhancing the occurrence of redox reactions [65]. Typically, an increase in reaction temperature improves the performance of photocatalysts in the degradation of dyes as well as the kinetic reaction [66]. For instance, Velidandi et al. [67] found that the degradation of 500 mg/L RhB and MO in both single and mixture systems by 10  $\mu\text{L}$  of Ag-AgCl nanoparticles exceeded 95% when the temperature increased from 40°C to 60°C. Furthermore, the results show that the further raising of the reaction temperature leads to a reduction in reaction time in order to achieve the maximum removal rate.

Bousalah et al. [58] also demonstrated the positive impact of temperature on the photodegradation of 300 mg/L of Indigotine dye by the photo-Fenton process. As the temperature increased from 20°C to 35°C, the photodegradation efficiency increased from 26% to 100% after 5 min of light irradiation. Moreover, their report has proven that less reaction time was required to complete the removal of Indigotine when the reaction temperature increased. Furthermore, Usman et al. [68] noted a similar trend as Bousalah et al. [58]. When the temperature rose from 20°C to 35°C, the degradation percentage of 20 ppm bromophenol blue (BPB) by 0.6 g/L of Fe<sub>3</sub>O<sub>4</sub>/rGO escalated from 91.87% to 98.27%, and the rate constant increased from 0.0544 min<sup>-1</sup> to 0.0776 min<sup>-1</sup>. In the same way, when the photodegradation of 200 mg/L MB by 0.1 g of ZnO-rGO with increased reaction temperature from 30°C to 50 °C, the rate constant increased from 0.026 min<sup>-1</sup> to 0.049 min<sup>-1</sup> [69]. This is attributed to the enhanced generation of •OH radicals, thereby accelerating the degradation rate. However, when the temperature continues to increase beyond the optimal temperature, it can have a negative impact on the photodegradation of the dye. This situation was reported by Barakat et al. [70] where the rate of photodegradation of 10 ppm MB by 0.5 wt% Ag-TiO<sub>2</sub> increased from 0.025 mg/min (5°C ) to 0.0313 mg/min (15°C), and then progressively decreased to 0.0181 mg/min when the temperature was raised to 55°C. This can be the fact that the high temperature leads to the reduction of binding interaction between dye molecules and photocatalysts before the degradation process is completed [71].

The parameter of temperature is highly influential in determining the kinetics of the photodegradation process. The earlier mentioned evidence indicates that the photodegradation kinetic rate has a fluctuating trend, with a significant peak initially, and then gradually decreases as the temperature further increases after reaching a threshold. This trend suggests that studies on reaction temperature under various operating parameters should be prioritised in order to reduce the reaction time, thereby enhancing the efficiency of dye degradation.

## 2.6 Effect on oxidising and reducing agent

During the photocatalytic degradation process, oxidants (ozone, hydrogen peroxide, sodium persulphate, potassium bromate) and reducing agents (sodium borohydride) play a synergistic role in the photocatalytic degradation of dyes as they improve the performance of photocatalysts in dye degradation. When oxidising agents are added, a benign process occurs as ROS can be generated by direct and indirect oxidation to achieve the purpose of

dye degradation [72]. The role of the oxidising agent is to enhance the oxidation reaction during dye photocatalysis. Whereas when introducing reducing agents in photocatalysis, the dye undergoes reductive degradation, which is beneficial to the semiconductor in cleaving the chromophore and decomposing the large dye molecules into small molecules [73].

There are significant changes with the introduction of oxidants in the photodegradation process. Previous studies by Bahadorirad et al. [47] demonstrated that 7.5 mg of ZnSnO<sub>3</sub>@S-doped g-C<sub>3</sub>N<sub>4</sub> had the lowest photodegradation rate (< 5%) for DB1 in the absence of O<sub>3</sub>. Upon the addition of O<sub>3</sub>, the degradation percentage boosted to approximately 70%. According to the same source, the photocatalytic ozonation process increased the degradation rate of dyes by 2.6 times and 2.1 times compared to photocatalytic degradation and ozonation processes, respectively. These findings support the assertion that the presence of oxidants plays a critical role in photodegradation efficiency, as the presence of oxidants improves the generation of ROS, thereby increasing the oxidation of dyes, finally leading to a high degree of degradation of dye contaminants [74]. Moreover, the presence of oxidants reduces electron-hole recombination and acts as an electron scavenger during the photocatalytic degradation process [75, 76]. Despite this, they also pose potential environmental challenges due to the formation of toxic by-products, and they can impede the photodegradation process when overloading oxidants [77].

To address these challenges, many researchers have investigated the optimal concentration of oxidising agents for dye degradation, focusing on the concentration range of oxidants to prevent photodegradation from being hindered while maximising photodegradation efficiency [78–80]. In the presence of various ranges of O<sub>3</sub> flux, the degradation efficiency of Amaranth dye by 0.1 g/L of Cu-ZnO under UV irradiation has a fluctuation trend [81]. With the increase of O<sub>3</sub> flux (0.28 g/h–0.44 g/h), the degradation efficiency gradually improved. Hereafter, the degradation efficiency declined from 90% to 82.7% with a further increase of O<sub>3</sub> flux (0.57 g/h). Similarly, in the photocatalytic ozonation of 20 mg/L Reactive Red 120 and Reactive Yellow 145, Rajeswari & Poongodi [82] utilised 0.2 g/L of Sn-ZnO as the photocatalyst in the presence of O<sub>3</sub> (0–0.48 g/h), the COD removal rate increases. Subsequently increasing the dosage of O<sub>3</sub> resulted in a decrease in the COD removal effect. The upward trend of the photocatalytic efficiency can be explained by Henry's law, that is, the increase in the concentration of O<sub>3</sub> leads to an increase in the mass transfer rate of O<sub>3</sub> from gaseous to liquid state, thereby increasing the

mass transfer coefficient [83, 84]. Therefore, the reaction of  $O_3$  and photogenerated electrons in the conduction band increased, resulting in an increase in the degradation efficiency. However, the excess amount of  $O_3$  can be reacted with the  $\bullet OH$  radicals to form a less reactive ROS.

A recent study investigated the effect of  $H_2O_2$  on the degradation of acid orange 7 (AO7) by ZnO in the photocatalytic degradation process [85]. During the first 20 min of the reaction time, the degradation efficiency increased steadily from 64.8% to 78.9% when the  $H_2O_2$  concentration (0.208-1.25 mM) increased. At 40 min, the removal efficiencies of AO7 were 97.1% and 99.7% at  $H_2O_2$  concentrations of 0.208 mM and 1.25 mM, respectively. In contrast, a divergent trend has been indicated in the degradation of 10 mg/L MO by the photo-Fenton process at pH 2.5 [49]. A complete decolorisation was achieved at 1 mM of  $H_2O_2$  concentration, and the decolorisation rate was approximately 60% at 40 mM. This is attributed to the hole scavenging effects as well as the reaction of excess amounts of  $H_2O_2$  and  $\bullet OH$  radicals to produce hydroperoxyl ( $HO_2\bullet$ ) radicals [28]. The  $HO_2\bullet$  radical (1.70 V) has lower oxidising power compared to the  $\bullet OH$  radical (2.8 V) [86, 87]. Thus, the low oxidising power of radicals decreases the performance of dye degradation.

In addition, Wang et al. [23] have explored the degradation of 20 mg/L reactive red wastewater by  $Na_2S_2O_8$  with a concentration range of 0.5-2.5 mmol/L. The results of this study have indicated that the increased concentration of  $Na_2S_2O_8$  enhanced the photodegradation of reactive red. After 1.5 mmol/L of  $Na_2S_2O_8$ , the photodegradation rate increased slowly due to the self-scavenging effect. According to Cao et al. [88], in the absence of  $Na_2S_2O_8$ , the photodegradation rate of 15 ppm MB by 50 mg of  $BiVO_4$  under visible light was 51.4%. While a synergistic effect occurred in the presence of  $Na_2S_2O_8$ , offering a photodegradation efficiency of 69.2%. Moreover, there is a significant increment in photodegradation of MB, from approximately 70% to 100%, as the concentration of  $Na_2S_2O_8$  increased from  $10^{-5}$  to  $5 \times 10^{-4}$  M, and levelled off at  $10^{-3}$  M. This can be attributed to the trapping of  $SO_4^{\bullet -}$  and  $\bullet OH$  radicals [89].

Recent studies have demonstrated the low or no degradation of dye when sodium borohydride ( $NaBH_4$ ) was used alone [90, 91]. This is because  $NaBH_4$  acts as an electron donor and requires a relay system (catalyst) to assist in the transfer of electrons from the borohydride ion ( $BH_4^-$ ) to the dye [92]. Moreover, electrons generated by  $BH_4^-$  ions have an association effect, resulting in more negative charges on the surface of the catalyst,

thereby enhancing the adsorption of electrophilic dyes [93]. According to research by Kanchana & Vijayalakshmi [94], when metal nanoparticles (Cu, Ni, Ag) were used as photocatalysts to degrade CV, bromocresol green, and MB in the presence of 5% NaBH<sub>4</sub> (wt/v), resulting in a complete discolouration. Moreover, based on studies by Rubai et al. [95], a positive effect of the concentration of NaBH<sub>4</sub> in the photodegradation of 50 mg/L reactive red 120 by 0.1 g of ZnO and Fe<sub>2</sub>O<sub>3</sub> nanoparticles was determined. As the concentration of NaBH<sub>4</sub> (0.05–0.2 g) increased, the photodegradation percentage of Reactive Red 120 increased from 25% (ZnO) and 35% (Fe<sub>2</sub>O<sub>3</sub>) to 100%. This is due to the fast reduction of dye molecules [96].

Based on the aforementioned studies, it can be stated that the presence of oxidising and reducing agents provides a synergistic effect during the photocatalytic degradation process. A positive relationship between the concentration of oxidising or reducing agents and the photodegradation efficiency. However, the optimal dosage of oxidising or reducing agents needs to be investigated to obtain maximum photodegradation efficiency.

### *2.7 Summative insight on photocatalysis parameters*

In summary, the parameters mentioned above greatly influence the photodegradation of dye. There is no definition of which parameters are the best. As every parameter is interrelated with the dye photocatalysis. The dye photocatalysis is highly influenced by the parameters discussed above, such as the photon energy given by light intensity affecting the adsorption of photons by the semiconductor photocatalyst; the adequate amount of photocatalyst allowing better performance of photodegradation; the pH of the solution significantly impacting the dye photocatalysis by adsorption dynamic and ROS generation; the appropriate initial concentration of dye permitting the passage of photons; a proper setting of reaction temperature enabling the increment of kinetic energy of dye particles; and the oxidising and reducing agents enhancing the redox reaction during the photodegradation. Refinement of these parameters can profoundly improve the efficiency of dye photocatalysis. Table 2 illustrates the various photocatalysis processes by summarising the optimal operating conditions and their photocatalytic performance. Different optimal conditions achieved the superior performance of the photocatalyst with the removal percentage of more than 90%.



Table 2: Comparison of the optimal conditions for different photocatalysis processes

Photocatalysis	Photocatalyst	Dye pollutant	Optimal condition	Photodegradation percentage (%)	References
Photocatalytic degradation	rGO	Indigo Carmine	Light source: Sunlight pH =10 Catalyst dosage: 0.055 g [Dye]= 25 ppm	98.74	[97]
		Neutral Red	Degradation time: 200 min	97.56	
Photocatalytic degradation	CuS nanoparticles	Methylene Blue	Light source: Sunlight	90.29	[24]
		Rhodamine B	Catalyst dosage: 0.03 g	69.23	
		Eosin Y	[Dye]= $2 \times 10^{-5}$ M	91.97	
		Congo Red	Degradation time: 240 min	60.35	
Photocatalytic ozonation	TiO <sub>2</sub> -Fe-Zeolite	Acid Red	Light source: UV light (10 W) pH = Neutral Catalyst dosage: 0.3 g/L (TiO <sub>2</sub> ); 20% (Fe-Zeolite) [Dye]: 100 ppm Degradation time: 5 min Ozone flow rate: 100 mg/h	99.00	[57]
Photocatalytic ozonation	Fe <sub>2</sub> O <sub>3</sub> /MoS <sub>2</sub>	Acid Blue 113	Light source: Visible light pH= 6.4 Catalyst dosage: 0.02 g [Dye]: 25 ppm Degradation time: 45 min Ozone flow rate: 0.2 g/l•h	99.00	[35]

\*[Dye] refers to the initial concentration of dye.

Table 2: (Continued)

Photocatalysis	Photocatalyst	Dye pollutant	Optimal condition	Photodegradation percentage (%)	References
Photo-Fenton	Fe <sub>3</sub> O <sub>4</sub> /α-Fe <sub>2</sub> O <sub>3</sub>	Methylene Blue	Light source: Mercury lamp (450 W) pH=2 Catalyst dosage: 1 g/L [Dye]: 50 ppm	99.00	[48]
		Congo Red	Degradation time: 12 min (MB); 8 min (CR) [H <sub>2</sub> O <sub>2</sub> ]: 25 mM	99.00	
Photo-Fenton	FeSO <sub>4</sub> •7H <sub>2</sub> O	Indigotine	Light source: Visible lamp (200 W) pH=3 Catalyst dosage: 0.125 mM [Dye]: 300 ppm Degradation time: 10 min [H <sub>2</sub> O <sub>2</sub> ]: 1.3 mM	100.00	[58]

\*[H<sub>2</sub>O<sub>2</sub>] refers to the concentration of hydrogen peroxide.

### 3. Mechanism of photocatalytic degradation process

In the photocatalytic degradation process, ROS plays an important role in studying the mechanisms. High reactive of ROS are generated during the beginning of the process, for instance, superoxide anions ( $O_2^-$ ), hydroxyl radicals ( $OH \cdot$ ), sulphate radicals ( $SO_4^{\cdot-}$ ), and singlet oxygen ( $^1O_2$ ) [98]. The ROS has strong redox properties, making them powerful oxidants and scavenging pollutants in the mineralisation process of organic pollutants. Ultimately, the mineralised products which are carbon dioxide ( $CO_2$ ) and water ( $H_2O$ ) have less impact on the environment. According to He et al. [99], during the photocatalytic degradation process, the interaction between the ROS and organic pollutants can be summarised in three key stages, including initiation, propagation, and termination phases (Figure 1). In general, ROS are generated via the promotion of the initiator and simulator in the initiation phase, followed by the immediate reaction of high reactive ROS on dye molecules in the propagation stage. Eventually, the disproportionation reaction occurs in the termination phase. The initiators such as  $O_3$ ,  $H_2O_2$ ,  $Na_2S_2O_8$ , and  $NaBH_4$  play a role in promoting the generation of ROS, whereas light irradiation and temperature serve as external simulators in enhancing the production of ROS.

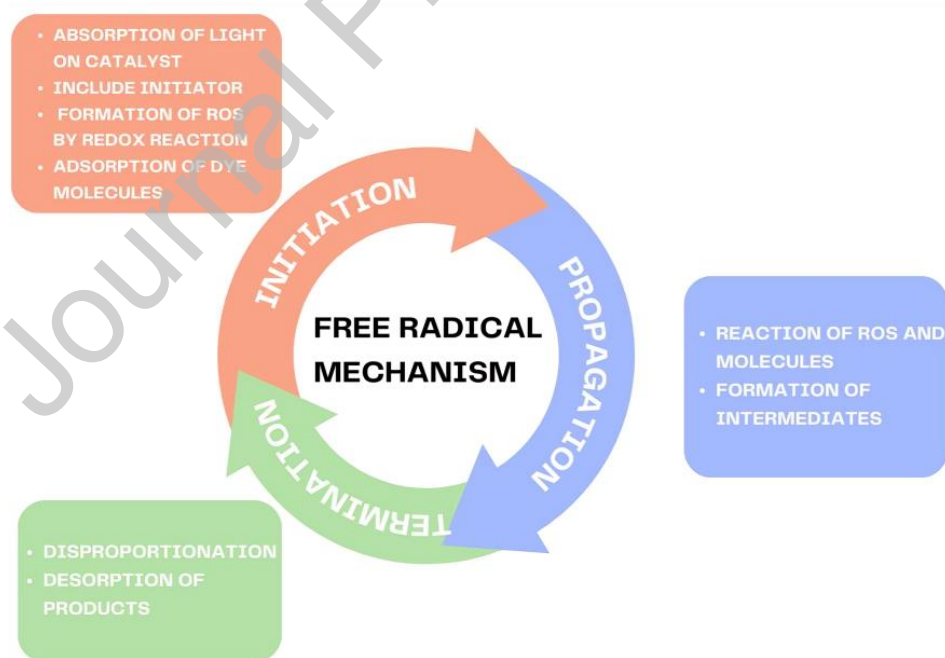
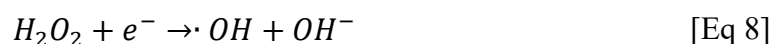
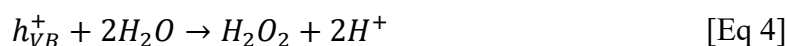


Figure 1: The free radical mechanism.

Photocatalytic degradation, also known as photocatalysis, is categorised into two categories: homogeneous photocatalysis and heterogeneous photocatalysis. Homogeneous photocatalysis is a degradation process in which the reactants and photocatalysts are in the

same medium [100]. Meanwhile, heterogeneous photocatalysis is a process in which the photocatalysts have different phases from the reaction medium, are activated by absorbing light, and then degrade organic pollutants into less harmful products. By introducing the oxidising agent in the photocatalysis process, a synergetic effect occurs, which enhances the generation of ROS, thereby improving the photocatalysis process [101].

In heterogeneous photocatalysis, various semiconductors have been employed as photocatalysts that facilitate the degradation of dyes into small fragments such as CO<sub>2</sub> and H<sub>2</sub>O. The semiconductor photocatalysts possess varying band gap sizes for the absorption of light. For instance, TiO<sub>2</sub>, ZnO, SnO<sub>2</sub>, and CuO are semiconductors that have been widely studied as photocatalysts, with bandgap energies of approximately 3.2 eV, 3.4 eV, 3.6 eV, and 1.9 eV, respectively [102–105]. Generally, when light with sufficient energy strikes the surface of a photocatalyst, electrons in the valence band absorb photon energy and cross the forbidden band to the conduction band [Eq 1]. This process is known as photoexcitation. The photogenerated holes in the valence band oxidise the hydroxyl ion (OH<sup>-</sup>) and H<sub>2</sub>O molecules to form •OH radical [Eq 2-4]. Conversely, photoinduced electrons in the conduction band have reducing properties that reduce the dissolved oxygen (O<sub>2</sub>) to undergo a series of reactions to gain ROS [Eq 5-8] [106]. The generated •OH radicals oxidise organic pollutants to produce intermediates and compound fragments, which are then further oxidised to form final products (CO<sub>2</sub> and H<sub>2</sub>O).



Homogeneous photocatalysis, such as photo-Fenton, photo-ozonation, and photo-oxidation, where the photocatalysts and dye pollutants have the same state of matter. Iron is a transition metal used as the photocatalyst in the photo-Fenton process. Initially, the trivalent ferric ions (Fe<sup>3+</sup>) absorb light energy to reduce to divalent ferric ions (Fe<sup>2+</sup>) [Eq 9]. The Fe<sup>2+</sup> ions then interact with H<sub>2</sub>O<sub>2</sub> to form OH<sup>-</sup> ions and •OH radicals and the ferric

ions return to divalent, which are ready to absorb more light for the photodegradation process [Eq 10]. The generated  $\bullet\text{OH}$  radicals then decompose organic dyes into intermediates, then  $\text{CO}_2$  and  $\text{H}_2\text{O}$  [Eq 13] [48]. However, the difficulties of recycling the iron ions in the photo-Fenton process limit the overall sustainability of the process [107]. In order to ensure the sustainability of photocatalysts, supporting materials are introduced for the immobilisation of ferric ions. Gou et al. [108] studied the heterogeneous ( $\text{MoS}_2@\text{Fe}/\text{H}_2\text{O}_2/\text{UV}$ ) photo-Fenton processes, in which  $\text{MoS}_2$  as the supporting material plays a crucial role in the adsorption of UV light [Eq 11]. The photogenerated  $h^+$  undergoes water ionisation with water molecules to generate  $\bullet\text{OH}$  radicals as mentioned above [Eq 3]. Whereas photogenerated  $e^-$  reduced  $\text{Fe}^{3+}$  ions to  $\text{Fe}^{2+}$  ions [Eq 12], and then decomposed  $\text{H}_2\text{O}_2$  to produce  $\bullet\text{OH}$  radicals [Eq 10].



When  $\text{O}_3$  is used in photocatalysis, the process is called photocatalytic ozonation.  $\text{O}_3$  acts as an initiator to generate ROS, enhancing the photodegradation process. In homogeneous photocatalysis, only photo-ozonation occurs with the presence of  $\text{O}_3$ , while heterogeneous photocatalysis involves both photo-ozonation and photocatalytic ozonation. The mechanism of photo-ozonation can be divided into two types: (i) direct and (ii) indirect ozone reactions, which are highly dependent on the reaction environment. Direct reaction is the main pathway under acidic conditions, while indirect ozonation is predominant under alkaline conditions [109]. The alone  $\text{O}_3$  directly electrophilically attacks organic pollutants or performs indirect photo-ozonation to generate  $\bullet\text{OH}$  radicals [Eq14-16].

Photo-ozonation:



In photocatalytic ozonation,  $\text{O}_3$  is primarily adsorbed on the surface of the photocatalyst. Herein, photocatalyst acts as a medium for electron mass transfer. Initially, the photogenerated  $e^-$  [Eq 1] is captured by  $\text{O}_3$  to generate ozonide radicals ( $\text{O}_3^-$ ) [Eq 17]. This

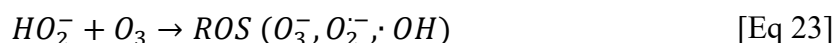
shows that the  $O_3$  acts as a scavenger to prevent the recombination of electron-hole pairs. Then, protonation of  $O_3^-$  [Eq 18-19] and oxygen ionosorption [Eq 5-8] take place [78]. During the protonation process,  $O_3^-$  radicals interact with hydrogen ions ( $H^+$ ) to form hydroxyl superoxide anion ( $HO_3^-$ ), then decompose into  $O_2$  and  $\bullet OH$  radicals.

An adequate number of oxidants can generate high amounts of  $\bullet OH$  radicals. Nonetheless, excess amounts of oxidants may negatively affect the photodegradation of dye. When an intensive amount of  $O_3$  is present in the photocatalysis process, the decomposition of  $O_3$  will take place [Eq 20-21]. The overage of  $O_3$  reacts with  $\bullet OH$  radicals, forming  $O_2$  and hydroperoxyl radicals ( $HO_2^\bullet$ ), then undergoes a reversible reaction to form superoxide anions ( $O_2^-$ ) and  $H^+$  ions. Furthermore, photocatalytic ozonation also highly relies on environmental conditions. Ozone decomposition is preferably favoured under alkaline conditions. Since the high concentration of  $OH^-$  ions may be the initiator of ozone decomposition, secondary oxidants are formed, which have weaker oxidising properties than  $\bullet OH$  radicals. [Eq 22-23] [46]. The generated ROS are then entered into the propagation and termination phase to produce  $CO_2$  and  $H_2O$ . Figure 2 illustrates the mechanism of photocatalytic degradation, photocatalytic ozonation, and photo-Fenton processes.

Photocatalytic ozonation:



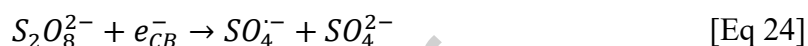
Ozone decomposition:



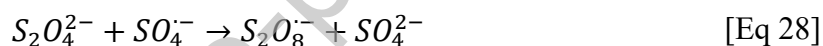
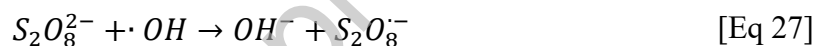
Moreover, in photocatalytic oxidation,  $Na_2S_2O_8$  and  $H_2O_2$  are also extensively utilised as oxidising agents in the process of dye degradation. When  $Na_2S_2O_8$  is added to the photocatalytic process,  $Na_2S_2O_8$  is dissociated in water to form sodium ion ( $Na^+$ ) and persulphate ion ( $S_2O_8^{2-}$ ). The  $S_2O_8^{2-}$  ion has a similar role as  $O_3$  as a scavenger of  $e^-$  of the conduction band, by trapping it to generate  $SO_4^{\bullet -}$  radicals [Eq 24]. Besides, the photolysis of  $S_2O_8^{2-}$  ion to generate  $SO_4^{\bullet -}$  radical [Eq 25]. The generated  $SO_4^{\bullet -}$  radicals are then

reacting with  $H_2O$  molecules to form  $\bullet OH$  radicals and sulphate ions ( $SO_4^{2-}$ ) [Eq 26] [96, 110]. Nevertheless, the concentrated  $S_2O_8^{2-}$  ions react with generated radicals ( $\bullet OH$  and  $SO_4^{\cdot-}$ ) to form  $S_2O_8^{\cdot-}$  radicals [Eq 27-28]. Also, the scavenging effect occurs when rich amounts of  $SO_4^{\cdot-}$  radicals are present [Eq 29-30] [110]. Likewise, when there is a high concentration of  $H_2O_2$  in the reaction environment,  $H_2O_2$  decomposes and eventually form  $O_2^{\cdot-}$  anions [Eq 31-32]. This is attributed to the higher oxidation-reduction potential of  $\bullet OH$  (2.8 V) and  $SO_4^{\cdot-}$  (2.6 V) radicals compared to  $O_3$  (2.07 V),  $H_2O_2$  (1.76 V), and  $S_2O_8^{2-}$  (2.01 V) [96, 111–113].

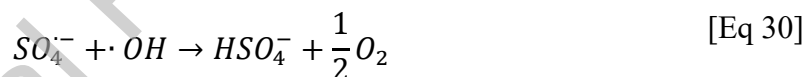
Photocatalytic oxidation by  $S_2O_8^{2-}$ :



Entrapment of  $\bullet OH$  and  $SO_4^{\cdot-}$ :



Scavenging of  $SO_4^{\cdot-}$ :



$H_2O_2$  decomposition:



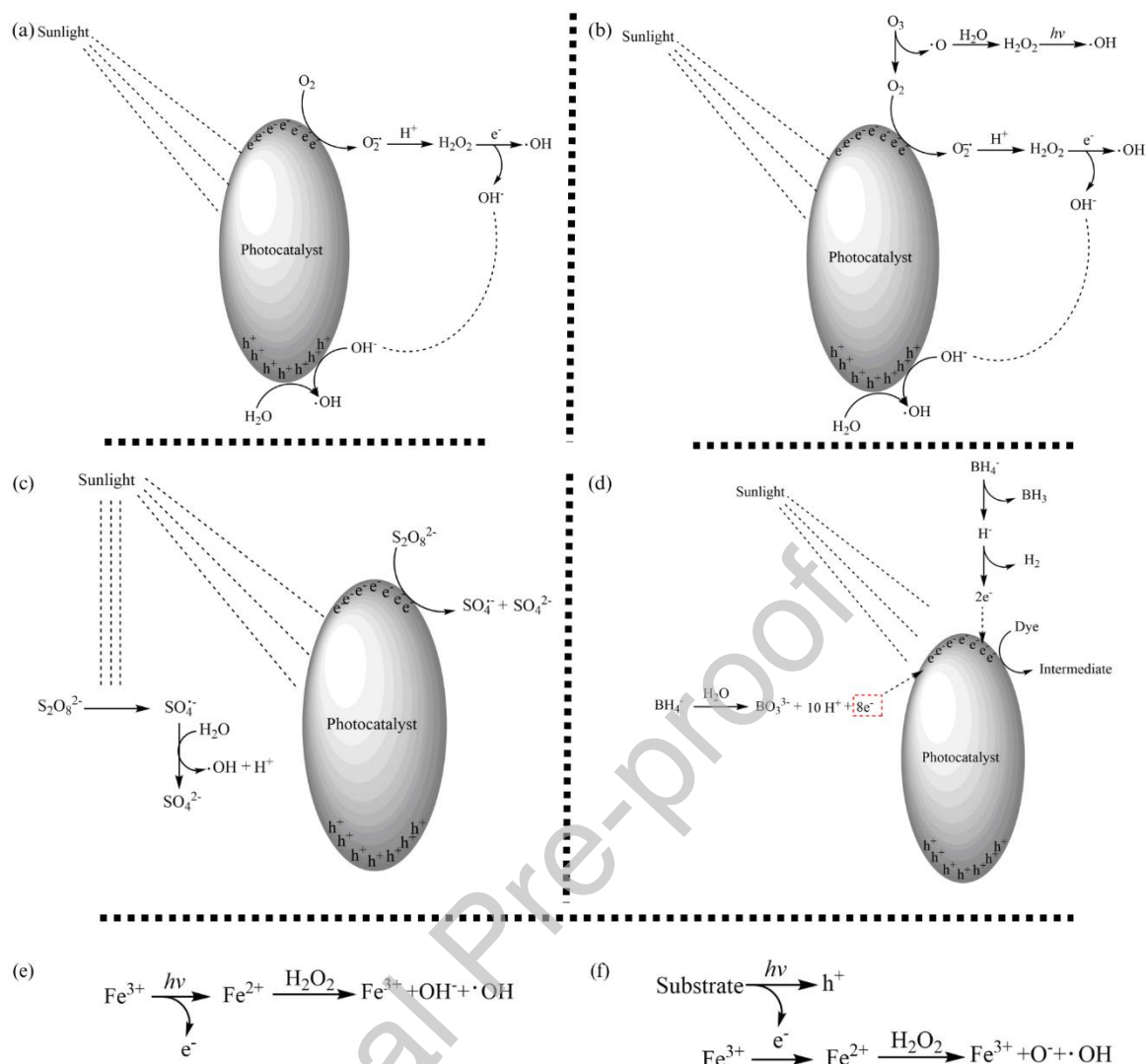
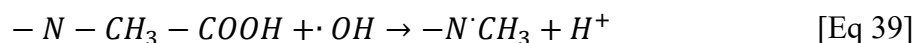
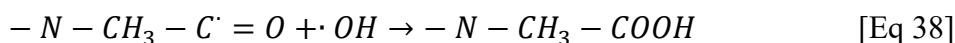
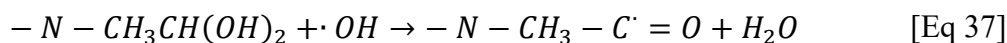
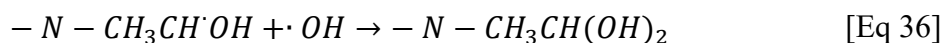
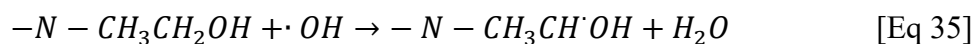
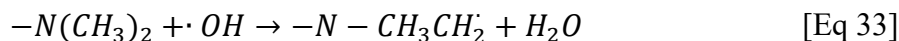


Figure 2: Mechanisms of (a) photocatalytic degradation, (b) photocatalytic ozonation by  $\text{O}_3$ , (c) photocatalytic ozonation by  $\text{Na}_2\text{S}_2\text{O}_8$ , (d) photocatalytic reduction, (e) photo-Fenton (homogeneous), (f) photo-Fenton (heterogeneous).

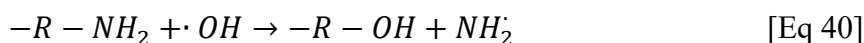
After the ROS radicals are generated, they enter the propagation and termination stages, which involve the redox reaction between ROS and the dye. According to Saha et al. [114], the degradation of organic dyes by demethylation, ring shortening, and ring-opening via redox reaction. Initially, the generated  $\cdot\text{OH}$  radical attacks the methyl group, forming alcohols, aldehydes, and carboxylic acids, and finally captures the H atom [Eq 33-39]. Next, Equations 40 to 42 demonstrate the reaction mechanism between the  $\cdot\text{OH}$  radical and the aromatic amine of dye. Moreover, oxidation of sulphur-containing species of dyes occurs through the attack of  $\cdot\text{OH}$  radicals [Eq 43-46]. From the perspective of the reaction mechanism, inorganic ions such as ammonium ions ( $\text{NH}_4^+$ ) and sulphate ions ( $\text{SO}_4^{2-}$ ) are generated.



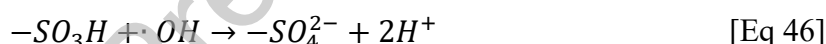
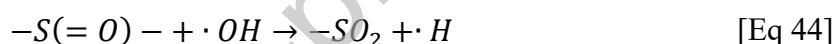
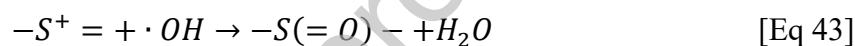
Demethylation:



Ring shortening:

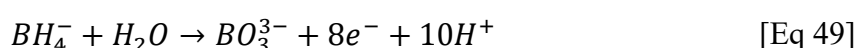


Ring-Opening:



Sodium borohydride ( $\text{NaBH}_4$ ) serves as a reducing agent in photocatalytic degradation. In photocatalytic reduction degradation,  $\text{NaBH}_4$ , dye molecules, and semiconductor photocatalysts act as nucleophiles, electrophiles, and relay systems, respectively [93, 115]. According to Kanchana & Vijayalakshmi [94], this reaction could be defined by the Eley-Rideal (ER) adsorption mechanism. Initially, the  $\text{BH}_4^-$  ions adsorbed on the semiconductor photocatalyst via electrostatic attraction. Then,  $\text{BH}_4^-$  ions are dissociated to form borane ( $\text{BH}_3$ ) and hydride ions ( $\text{H}^-$ ), and finally release electrons [Eq 47-49], which are accepted by the photocatalyst. As a relay system, photocatalysts act as substrates for reactions between electron acceptors and donors [116]. The electron is then donated to absorbed dye molecules to undergo a reduction process [117]. After the reduction of the dye molecules is completed, desorption occurs.

Dissociation of borohydride ions,  $\text{BH}_4^-$ :



#### 4. Proposed degradation pathway

After exploring the parameters that influence the effect of dye photodegradation and the hypothesised mechanisms of dye photodegradation upon the addition of oxidising and reducing agents, it is necessary to consider the production of intermediates and end products of the process. In this context, this section will focus on the techniques being used for studying the intermediates produced during the photodegradation, providing insight into the degradation pathway of the photodegradation process.

In general, the chemical structure of synthetic dyes consists of skeletons (benzene, naphthalene, and anthracene), auxochromes (hydroxyl and amine groups), chromophores (nitroso, azo, alkene, and carbonyl groups), and solubilising groups (sulfonic groups) [118, 119]. These groups are frequently targeted in the degradation process, transforming them into simpler or more desirable compounds. Nonetheless, the intermediates produced during photodegradation may pose a risk affecting the aquatic food chains [120]. Analytical techniques such as spectroscopy (Fourier Transform Infrared Spectroscopy and UV-vis spectrophotometry) and integrated techniques (HPLC-MS, GC-MS, LC-MS, and UHPLC-MS) have been utilised to identify the intermediates during photocatalysis prior to proposing a degradation pathway for dyes. Both spectroscopy and chromatography are employed for periodic monitoring of the emergence of new substances or the change in dye molecule concentration over time.

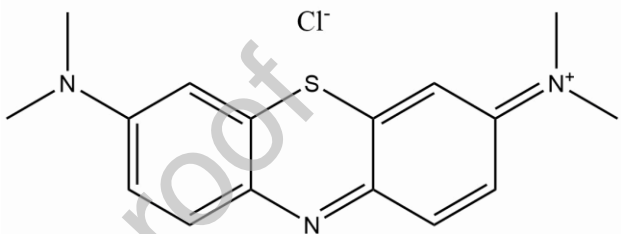
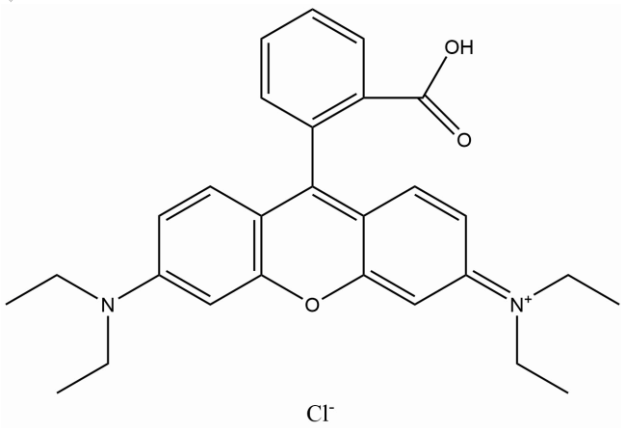
##### 4.1 Fourier Transform Infrared Spectroscopy (FTIR)

FTIR spectroscopy is used to analyse the changes in the functional groups of dye molecules during the photocatalytic process by comparing the peaks that appear on the FTIR spectrum before and after photodecolouration. New bands appear after the photodegradation, indicating the cleavage of bonds and the formation of new fragments. The diminishing peak intensity represents the weakening properties of certain functional groups. Thus, it can be interpreted that the bonds at the functional groups are broken, resulting in a reduction in the concentration of the functional groups.

MB is a cationic thiazine dye, where the heterocyclic aromatic consists of an N-S conjugated system that acts as a chromophore to provide a blue colour, and amine groups (-NR<sub>2</sub>) are the auxochromes, improving the colour intensity. Table 3 and Table 4 illustrate the structure of MB as well as its FTIR spectra. Based on Ovchinnikov et al.'s report [121], the structural property of MB (Table 4) consists of overlapping O-H and N-H stretching

(3700-3200  $\text{cm}^{-1}$ ), asymmetric and symmetric C-H stretching (3000-2840  $\text{cm}^{-1}$ ), skeletal stretching vibrations of C=C (1650-1566  $\text{cm}^{-1}$ ) and C=N bands (1342-1266  $\text{cm}^{-1}$ ), stretching vibrations of C-N (1342-1266, 1250-1020  $\text{cm}^{-1}$ ) and C=S<sup>+</sup> (~1350  $\text{cm}^{-1}$ ) bonds heterocycles as well as bending vibrations of C-H bonds (880-770  $\text{cm}^{-1}$ ). The O-H stretching involves interaction with nitrogen atoms allocated in the heterocycle and dimethylamino group.

Table 3: The structure and molecular weight of MB and RhB.

Dye	M.W.	$\lambda_{\text{max}}$	Structural
Methylene blue (MB)	319.85 g/mol	664 nm	
Rhodamine B (RhB)	479.02 g/mol	546 nm 567 nm	

\*M.W. refers to molecular weight;  $\lambda_{\text{max}}$  refers to maximum wavelength

Table 4: The FTIR spectra of MB [121].

Frequency range ( $\text{cm}^{-1}$ )	Assignment
3560-3170	Overlapping of stretching vibration of O-H bonds and N-H bonds
3000-2840	Asymmetric and symmetric stretching vibration of C-H bonds in alkane group
1650-1566	Stretching vibration of C=C in cyclic alkene group
~1350	Stretching vibration of C=S <sup>+</sup> bonds
1342-1266	Stretching vibration of C-N bonds in aromatic amine

Frequency range (cm <sup>-1</sup> )	Assignment
1250-1020	Stretching vibration of C-N bonds in amine groups
880-770	Bending vibration of C-H bonds
850-550	Stretching vibration of C-Cl bonds in halo compound
720-680	Benzene derivatives

Table 6 exhibits the FTIR spectra of MB and RhB after photodegradation and their assignments. As reported by Majeed et al. [122], a comparison of FTIR spectra was studied before and after the photodegradation of MB. After MB photodegradation, multiple new peaks appeared in the 3600-2800 cm<sup>-1</sup> region. These peaks represent the overlapping bands of N-H and O-H (3527 and 3406 cm<sup>-1</sup>) as well as the N-H stretching and bending (3209 and 3026 cm<sup>-1</sup>). An adsorption band at 1753 cm<sup>-1</sup>, is attributed to the C-N stretching vibration. On the authority of Mohamadi & Ghorbanali [123], after the photodegradation of MB by CeO<sub>2</sub>@GS sponge, numerous absorption peaks were diminished, and new characteristic peaks were discovered in the spectrum of degraded MB. Strong peaks around 3417 cm<sup>-1</sup> and 1638 cm<sup>-1</sup> correspond to the characteristic of water, whereas the peak at 1028 cm<sup>-1</sup>, indicates the presence of C-N bonds from aliphatic amine groups. Furthermore, a peak near 2074 cm<sup>-1</sup> indicates a stretching band of N=C=S, confirming the presence of the isothiocyanate complex. Alvarado et al. [124] reported that the MB was degraded by ZnO nanoparticles to form products such as secondary alcohol, thiocyanate complexes, nitro compounds, and water. The secondary alcohol was characterised by absorption peaks around 2990-2900 cm<sup>-1</sup>, 1480-1410 cm<sup>-1</sup>, and 1090-1000 cm<sup>-1</sup>. The complexes of thiocyanate and isothiocyanate exhibited peaks near 2370-2230 cm<sup>-1</sup> and 2050 cm<sup>-1</sup>, respectively. In addition, strong peaks appeared in the 3600-3200 cm<sup>-1</sup> region, associated with intermolecular O-H stretching, confirming the existence of water molecules.

RhB, a xanthene dye, has a structure consisting of a planar heterocyclic skeleton incorporating "O". RhB is a carcinogenic and mutagenic organic compound, which undergoes phototoxic reactions to produce intermediates that are harmful to the living organism. Table 5 presents FTIR spectra of pure RhB [125]. The bands around 3500 cm<sup>-1</sup> and 3300 cm<sup>-1</sup>, were associated with the O-H stretching from alcohol and carboxylic group, respectively. These peaks indicate the presence of the carboxylic and -OH groups involved in intermolecular hydrogen bonding with water molecules. In addition, distinct peaks at 3100 cm<sup>-1</sup> and 2900 cm<sup>-1</sup>, correspond to the stretching vibrations of C-H from alkene and alkane groups. Absorption around 1600 cm<sup>-1</sup> is associated with C=O stretching vibration, which further supports the presence of the carboxylic group in the RhB structure. Bands

near  $1220\text{ cm}^{-1}$  indicate the occurrence of C-O stretching, which is integral to the dye's structural properties.

Table 5: The FTIR spectra of RhB [126][127].

Frequency range ( $\text{cm}^{-1}$ )	Assignment
~3500	Stretching vibration of O-H bonds from alcohol group
~ 3300	Stretching vibration of O-H bonds from carboxylic group
~ 3100	Stretching vibration of C-H bonds from alkene group
~ 2900	Stretching vibration of C-H bonds from alkane group
~ 1600	Stretching vibration of C=O from carboxylic group
~ 1220	Stretching vibration of C-O from ether group
~ 820	Bending vibration of C-H out of plane

Zhu et al. [128] reported that bands of intermediate after photodegradation of RhB by  $\text{TiO}_2/\text{cellulose}$  microsphere were at  $3390\text{ cm}^{-1}$  and  $3183\text{ cm}^{-1}$  (N-H stretching),  $2956\text{ cm}^{-1}$ ,  $2924\text{ cm}^{-1}$ , and  $2851\text{ cm}^{-1}$  (C-H stretching),  $1711\text{ cm}^{-1}$  (C=O stretching),  $1650\text{ cm}^{-1}$  and  $1456\text{ cm}^{-1}$  (C-H bending), and  $1370\text{ cm}^{-1}$  (O-H bending). In accordance with P. Chen et al. [83] and Ma et al. [127], the frequency band of O-H stretching of RhB is shifted toward lower frequency after the photodegradation, from  $3575\text{ cm}^{-1}$  to  $3320\text{ cm}^{-1}$  and  $3440\text{ cm}^{-1}$  to  $3240\text{ cm}^{-1}$ , respectively. This corresponds to the transition from intermolecular hydrogen bonding interactions with H-N and H-N-C groups before photodegradation to intermolecular hydrogen bonding interactions with O-H and C-H groups after photodegradation, illustrating the de-ethylation process [129].

The findings from the FTIR analysis provide valuable insights into the difference in chemical characteristics between pure dye and intermediate after photodegradation. In spite of that, superficial information about the intermediate can be obtained from FTIR analysis, attributed to the several superimposed pinnacles [130]. Thus, the auxiliary of other spectroscopy or mass spectrum analysis supports the validation of intermediates and end products during photodegradation.

Table 6: The FTIR spectral of dye and its intermediates of photodegradation and its assignment.

Dye	Reference	Wavenumber (cm <sup>-1</sup> )	Assignment
Methylene blue	[122]	3527, 3406, 3308	Stretching vibration band of O-H/ Stretching vibration band of N-H
		3209, 3026	Stretching & bending vibration of -N-H from amide group
		2916	Stretching vibration of C-H bonds in methylene
		1753	Heterocyclic aromatic C-N bonds
		1654	Stretching vibration of C=O bonds
		1474	Stretching vibrations of C-N bonds in aromatics amines/ Bending of O-H groups
		1319	Symmetric and asymmetric stretching vibration of -CH <sub>3</sub> groups / C=N group
		1120	Stretching vibration within the aliphatic chain
		870	Bending vibration of C-H in-plane
	[123]	3417	Stretching vibration of O-H bonds from alcohol group
		2074	Stretching vibration of N=C=S bonds from isothiocyanate groups
		1638	Stretching vibration of C=C bonds from alkene groups
		1264	Stretching vibration of C-O bonds from ester groups
		1028	Stretching vibration of C-N bonds from amine groups
	[124]	710	Bending vibration of C=C bonds from alkene groups
3600-3200, 2990-2900		Stretching vibration of O-H bonds	
2370-2230		Stretching vibration of N=C=O bonds	
~2050		Stretching vibration of N=C=S bonds	
1630-1600		Stretching vibration of C=C bonds from conjugated alkene groups	
1480-1410		Bending vibration of C-H bonds in alkane groups	
1390-1280	Stretching vibration of N-O bonds from nitro compounds		
1090-1000	Stretching vibration of C-O bonds from secondary alcohol		

Table 6: (Continued)

Dye	Reference	Wavenumber (cm <sup>-1</sup> )	Assignment
RhB	[128]	3390, 3183	Stretching vibration of N-H from amines
		2956, 2924, 2851	Stretching vibration of C-H from alkene
		1711	Stretching vibration of C=O from carboxylic groups
		1650	Bending vibration of C-H from aromatic compounds
		1456	Bending vibration of C-H from alkane
		1370	Bending vibration of O-H from phenol
	[131]	3320	Stretching vibration of O-H from alcohol
	[127]	3240	Stretching vibration of O-H bonds

#### 4.2 UV-vis spectrophotometry

UV-vis spectroscopy is commonly used in monitoring the changes in dye concentration during photocatalysis. Changes in concentration can be judged by observing changes in the maximum wavelength absorbance of the dye. The absorbance decreased with the prolongation of reaction time during the photocatalytic process, indicating a decrease in dye concentration. Besides, the decomposition process of dyes can be determined by analysing the shifting of absorption peaks using UV-vis spectroscopy [132].

MB has four prominent absorption peaks at 246, 300, 613, and 665 nm, in particular, the peak at 664 nm is the most focused, as it represents the characteristic of the chromophore (central benzene ring), offering a blue colour in solution [133, 134]. As the decrease in absorbance of the peak at 664 nm, the decrease in the characteristic of the chromophore signifies the disruption of the benzene ring. As reported by Liu et al. [135], when the photodegradation of MB by g-C<sub>3</sub>N<sub>4</sub>, the absorption peak of MB shifted significantly from 663 nm to 609 nm at 80 min irradiation. Likewise, Nair et al. [136] found that there was a minor blue shift in the absorption peak of MB when it was photodegraded by TiO<sub>2</sub> and ZnO. Moreover, when MB was being photodegraded by nano-TiO<sub>2</sub> and nano-ZnO, new peaks appeared around 331 nm and 370 nm, respectively, resulting in the demethylation of MB molecules.

RhB, an N-alkylamine-containing dye, has a prominent characteristic peak of around 556 nm. Along the photocatalysis, the characteristic peak changes with time. According to Phuruangrat et al. [137], during the photodegradation of RhB by undoped CdS and Eu-doped CdS, a notably hypsochromic shift and a progressive decrease in the intensity of the absorption peak occurred. This is attributed to the de-ethylation of the N-ethyl group and disruption of chromophore structure leading to ring-opening [138, 139]. Similarly, J. Chen et al. [140] reported that in the presence of hydroxyl-group-modified g-C<sub>3</sub>N<sub>4</sub>, the absorption peak intensity significantly diminished concomitant with a slight blue shift (from 552 nm to 497 nm) under irradiation of visible light.

In summary, during the photocatalysis process, the transition in characteristic peaks of dyes provides superior insight into the degradation process (demethylation, de-ethylation, and ring-opening). Nonetheless, only conspicuous conjugated systems are able to be analysed by UV-vis spectrometry. As a result, to gain a more comprehensive understanding



of the characteristics of intermediates and products during the photocatalysis of dye, the integration of UV-vis spectrometry with other analytical techniques is essential.

#### 4.3 Integrated techniques

Integrated techniques of chromatography equipped with mass spectrometry are commonly used to determine the chemical characteristics of intermediates. Chromatography determines the interaction of the analysed compound with the stationary phase via retention time, whereas mass spectrometry determines the molecular weight of intermediates by the mass-to-charge ratio ( $m/z$ ). For analysing the intermediates generated during the photodegradation of dyes by chromatography-mass spectrometry, specific conditional setups are shown in Table 7. Typically, the degradation pathway of dyes can be summarised in 4 main steps, which are demethylation or de-ethylation, chromophore cleavage, opening ring, and mineralisation [33, 114, 141]. These steps have occurred by attacking ROS generated in the initiation phase [Eq 1-25].

In the degradation pathway of MB (Figure S2), two competing processes are proposed to occur simultaneously, namely demethylation or ring shortening. When demethylation is the initial step in MB degradation, the  $Csp^3-N$  bonds were ruptured to form Azure B ( $m/z$  270), Azure A ( $m/z$  256), Azure C ( $m/z$  242), and thionine ( $m/z$  228). According to the study by Martin & Leprince-Wang [142], Azure B was analysed when the reaction time for photodegradation was zero. This is due to the fact that the presence of impurities in MB or demethylation occurs when exposed to light. Nonetheless, Azure C and thionine were absent from the mass spectra of Saha et al.'s work [114]. This may be due to the rapid oxidation of these two compounds. Concurrently, the destruction of the benzene ring occurs, followed by ring shortening, in which the destruction of N-S heterocyclic group structure bonds. The intermediates produced in this process were the tricyclic and monocyclic compounds in Figure S1(d-o). These intermediates are further oxidised by  $\bullet OH$  radicals to form amine and amino/sulfonic acid-containing species as well as succinic acid. Ultimately, the intermediates are mineralised to produce non-toxic organic acids (acetic acid and oxalic acid) and mineralised inorganic substances ( $CO_2$ ,  $H_2O$ ,  $NO_3^-$ ,  $SO_3^-$ ,  $SO_4^{2-}$ ).

During the photocatalytic degradation of RhB, the generated ROS radicals, as mentioned above, react with the adsorbed RhB on the photocatalyst and undergo degradation processes, including N-de-ethylation, decarboxylation, and cleavage of the chromophore. Figure S3 shows the intermediates detected during the photocatalytic

degradation of RhB by LC-MS, LC-MS/MS, and GC-MS [141, 143–145]. Figure S3 (b-j) demonstrates the structure of intermediates of RhB after the amino group oxidation process, while Figure S3 (k-w) depicts the structural intermediates of RhB subsequent to the ring shortening. Based on these intermediates, the proposed RhB degradation pathway is shown in Figure S4, in which there are four possible pathways to degrade RhB into organic small molecules and inorganic compounds. The first possible route that has been proposed is progressive de-ethylation via an attack on  $\bullet\text{OH}$  radicals [141, 146]. The second route is assumed to occur under acidic conditions due to the presence of a high concentration of  $\bullet\text{OH}$  radicals. The chromophores of  $\text{RhB}^+$  molecules are disrupted, forming intermediates with  $m/z$  182 and 153 [143]. The third pathway postulated that the  $\text{RhB}^+$  molecules are attacked by  $\text{O}_2^-$  to form intermediates with  $m/z$  314, then further decomposed to generate a resorcinol compound ( $m/z$  110). The fourth route is initially de-ethylated to form an intermediate at  $m/z$  415 and then hydroxylated to form intermediates at  $m/z$  116 and 244 [145]. All the intermediates are then further oxidised, leading to ring shortening and ring opening, yielding aliphatic conjugated compounds and ultimately  $\text{CO}_2$  and  $\text{H}_2\text{O}$ .

In summarising the postulated degradation pathway of azo and xanthene dyes, the ROS preferentially attack the methyl ( $-\text{CH}_3$ ) or ethyl ( $-\text{CH}_2\text{CH}_3$ ), amino ( $-\text{NH}_2$ ), and sulphate ( $-\text{SO}_4^{2-}$ ) groups, resulting in demethylation, de-ethylation, deamination, and desulfonation. These steps have allowed the discolouration of dyes due to the destruction of chromophores and auxochromes of dyes. Whereas aromatic rings have more chemical stability, which makes them resistant to direct attack by ROS [147]. Therefore, ring opening comes after the demethylation or de-ethylation and ring shortening.

Table 7: The conditional setup of HPLC-MS, GC-MS, LC-MS, and UHPLC-MS.

Technique	HPLC-MS	GC-MS	LC-MS	UHPLC-MS
Reference	[148]	[149]	[150]	[33]
<b>Samples</b>	Methylene Blue	Basic Red 51	Direct Blue 1, Methyl Red, and Reactive Black 5	Rhodamine B and Methyl Orange
<b>Mobile phase/ Carrier gas</b>	A: 0.1% formic acid in water B: 0.1% formic acid in methanol	Helium gas	Acetonitrile: Water (70:30, v/v)	A: 0.1% formic acid in water B: 0.1% formic acid in acetonitrile
<b>Column type</b>	C 18 (2.1 m x 100 mm, 3 $\mu$ m)	HP5- MS capillary column (30 m x 0.25 mm, 0.25 $\mu$ m)	Capillary column Terra C18 (5 m x 100 mm, 0.22 $\mu$ m)	Synchronis C18 (100 x 2.1 mm, 1.7 $\mu$ m)
<b>Flow rate</b>	0.25 mL/min	1 mL/min	0.08 mL/min	0.4 mL/min
<b>Temperature control/programming</b>	40 °C	50 °C (for 1 min); 100 °C (20 °C/min for 1 min); 180 °C (10 °C/min for 1 min); 220 °C (5 °C/min for 5 min); 300 °C (10 °C/min for 5.5 min)	200 °C	30 °C
<b>Ionization technique</b>	ESI	EI (70 eV)	ESI	EI

\* EI refers to electron impact ionization; ESI refers to electrospray ionization

## 5. Conclusion

Photocatalysis is an advantageous advanced method for dye wastewater treatment. This is due to the end products being green and safe. This review emphasises the influence of environmental factors on photodegradation dye, the mechanism of photocatalysis, and intermediates formed in the degradation pathway. Evidently, by manipulating the operational parameters in accordance with the properties of photocatalysts, the performance of photocatalysis can be enhanced. In addition, the researchers postulated the ROS production mechanism when tuning parameters, such as the pH of the solution, oxidants, and reducing agents. Furthermore, a great comprehension of the dye degradation pathways was obtained by identifying the intermediates formed during the photocatalytic process using analytical techniques (FTIR, UV-Vis spectroscopy, chromatography). Based on the analysed intermediates by MS, the degradation pathway of dyes was proposed. It can be summarised that the complete degradation of azo or xanthene dyes undergoes four steps: demethylation or de-ethylation, ring shortening, ring opening, and mineralisation. This is attributed to the oxidation of ROS, which cleaves the chromophore, causing discolouration, destroying the aromatic ring, and eventually breaking the bonds of the aliphatic chain to obtain a smaller, safer molecule. There is still ongoing study on the intermediates and end products of photocatalysis to confirm the dye pollutant is completely mineralised and not only discoloured. Moreover, researchers endeavour to investigate photocatalysis in dye mixtures instead of single dyes, as the dye wastewater consists of multiple dyes. By studying the parameters of dye photocatalysis, the optimised conditions can be identified as the most suitable for implementation in the scaling-up process, thereby reducing the release of dye wastewater into water bodies. Additionally, investigating the mechanisms of photocatalysis and the pathways of photodegradation serves to confirm and optimise the complete mineralisation of dyes.

Over the past decade, the field of dye photocatalysis has predominantly concentrated on single dyes and intrinsic semiconductor photocatalysts. This foundational research has laid the groundwork for a deeper understanding of the photocatalytic mechanisms and their efficacy in dye degradation. However, recent studies have begun to shift their focus towards more complex systems, investigating binary dyes that better simulate real-dye wastewater scenarios, improved degradation efficiency and analysis of intermediates and end products, as well as doped semiconductor photocatalysts that offer enhanced performance and tailored properties. In consideration of future research directions, it is advisable that

subsequent endeavours expand the scope to encompass multiple dyes and real wastewater samples. This approach ensures that the developed photocatalytic processes are more applicable and effective in real-world environmental remediation. Additionally, it is imperative to investigate the synergistic effect of using both oxidising and reducing agents in dye photocatalysis. This combination could potentially reveal novel mechanisms and pathways, leading to the enhancement of degradation efficiency and broader applicability in wastewater treatment. Furthermore, it is essential for future studies to explore the scaling-up photocatalytic of real dye wastewater, particularly in maintaining efficiency and cost-effectiveness.

## **6. Acknowledgements**

The authors gratefully acknowledge the financial support provided by Universiti Sultan Abdullah Pahang, Malaysia under the Postgraduate Research Grant Scheme (PGRS230373).

## Reference

1. Hussain, T., Wahab, A.: A critical review of the current water conservation practices in textile wet processing. *J Clean Prod.* 198, 806–819 (2018).  
<https://doi.org/10.1016/J.JCLEPRO.2018.07.051>
2. Kant, R.: Textile dyeing industry an environmental hazard. *Nat Sci (Irvine)*. 2012, 22–26 (2011). <https://doi.org/10.4236/NS.2012.41004>
3. Li, C.J., Zhang, Y.J., Chen, H., He, P.Y., Meng, Q.: Development of porous and reusable geopolymer adsorbents for dye wastewater treatment. *J Clean Prod.* 348, 131278 (2022).  
<https://doi.org/10.1016/J.JCLEPRO.2022.131278>
4. Mcyotto, F., Wei, Q., Macharia, D.K., Huang, M., Shen, C., Chow, C.W.K.: Effect of dye structure on color removal efficiency by coagulation. *Chemical Engineering Journal.* 405, 126674 (2021). <https://doi.org/10.1016/J.CEJ.2020.126674>
5. Xiang, J., Wang, X., Ding, M., Tang, X., Zhang, S., Zhang, X., Xie, Z.: The role of lateral size of MXene nanosheets in membrane filtration of dyeing wastewater: Membrane characteristic and performance. *Chemosphere.* 294, 133728 (2022).  
<https://doi.org/10.1016/J.CHEMOSPHERE.2022.133728>
6. Elzahar, M.M.H., Bassyouni, M.: Removal of direct dyes from wastewater using chitosan and polyacrylamide blends. *Scientific Reports |.* 13, 15750 (2023).  
<https://doi.org/10.1038/s41598-023-42960-y>
7. Kheddo, A., Rhyman, L., Elzagheid, M.I., Jeetah, P., Ramasami, P.: Adsorption of synthetic dyed wastewater using activated carbon from rice husk. *SN Appl Sci.* 2, (2020).  
<https://doi.org/10.1007/s42452-020-03922-5>
8. Marszałek, J., Żyła, R.: Recovery of water from textile dyeing using membrane filtration processes. *Processes* 2021, Vol. 9, Page 1833. 9, 1833 (2021).  
<https://doi.org/10.3390/PR9101833>
9. Sonal, S., Mishra, B.K.: Role of coagulation/flocculation technology for the treatment of dye wastewater: Trend and future aspects. *Water Pollution and Management Practices.* 303–331 (2021). [https://doi.org/10.1007/978-981-15-8358-2\\_13](https://doi.org/10.1007/978-981-15-8358-2_13)
10. Gasmi, A., Ibrahim, S., Elboughdiri, N., Tekaya, M.A., Ghernaout, D., Hannachi, A., Mesloub, A., Ayadi, B., Kolsi, L.: Comparative study of chemical coagulation and electrocoagulation for the treatment of real textile wastewater: Optimization and operating cost estimation. *ACS Omega.* 7, 22456–22476 (2022).  
[https://doi.org/10.1021/ACSOMEGA.2C01652/ASSET/IMAGES/MEDIUM/AO2C01652\\_M024.GIF](https://doi.org/10.1021/ACSOMEGA.2C01652/ASSET/IMAGES/MEDIUM/AO2C01652_M024.GIF)
11. Ighalo, J.O., Omoarukhe, F.O., Ojukwu, V.E., Iwuzor, K.O., Igwegbe, C.A.: Cost of adsorbent preparation and usage in wastewater treatment: A review. *Cleaner Chemical Engineering.* 3, 100042 (2022). <https://doi.org/10.1016/J.CLCE.2022.100042>

12. Takkar, S., Tyagi, B., Kumar, N., Kumari, T., Iqbal, K., Varma, A., Thakur, I.S., Mishra, A.: Biodegradation of methyl red dye by a novel actinobacterium *Zhihengliuella* sp. ISTPL4: Kinetic studies, isotherm and biodegradation pathway. *Environ Technol Innov.* 26, (2022). <https://doi.org/10.1016/J.ETI.2022.102348>
13. Sonwani, R.K., Patel, D., Singh, A., Singh, R.S., Rai, B.: Intensified biodegradation of Congo red dye by mixed culture in a sequential bioreactor: Kinetics and phytotoxicity studies. *Indian J Exp Biol.* 61, (2023). <https://doi.org/10.56042/ijeb.v61i10.1686>
14. Ancy, K., Bindhu, M.R., Bai, J.S., Gatasheh, M.K., Hatamleh, A.A., Ilavenil, S.: Photocatalytic degradation of organic synthetic dyes and textile dyeing waste water by Al and F co-doped TiO<sub>2</sub> nanoparticles. *Environ Res.* 206, 112492 (2022). <https://doi.org/10.1016/J.ENVRES.2021.112492>
15. Li, W., Wang, Z., Li, Y., Ghasemi, J.B., Li, J., Zhang, G.: Visible-NIR light-responsive 0D/2D CQDs/Sb<sub>2</sub>WO<sub>6</sub> nanosheets with enhanced photocatalytic degradation performance of RhB: Unveiling the dual roles of CQDs and mechanism study. *J Hazard Mater.* 424, 127595 (2022). <https://doi.org/10.1016/J.JHAZMAT.2021.127595>
16. Qin, X., Zeng, X., Cheng, S., Xing, B., Shi, C., Yi, G., Nie, Y., Wang, Q., Zhang, C., Xia, H.: Preparation of double functional carbon-based ZnO derived from rape straw for dye wastewater treatment. *Journal of Water Process Engineering.* 52, 103588 (2023). <https://doi.org/10.1016/J.JWPE.2023.103588>
17. Fatima, S., Munawar, T., Nadeem, M.S., Mukhtar, F., Khan, S.A., Koc, M., Iqbal, F.: Boosted natural sunlight driven photodegradation of organic dyes using rGO anchored Pr/Cu dual-doped ZnO nanocomposite: Characterization and mechanistic insight. *Opt Mater (Amst)* 136, 113397 (2023). <https://doi.org/10.1016/J.OPTMAT.2022.113397>
18. Yasin, M., Saeed, M., Muneer, M., Usman, M., ul Haq, A., Sadia, M., Altaf, M.: Development of Bi<sub>2</sub>O<sub>3</sub>-ZnO heterostructure for enhanced photodegradation of rhodamine B and reactive yellow dyes. *Surfaces and Interfaces.* 30, 101846 (2022). <https://doi.org/10.1016/J.SURFIN.2022.101846>
19. Saini, D., Aggarwal, R., Sonker, A.K., Sonkar, S.K.: Photodegradation of azo dyes in sunlight promoted by nitrogen-sulfur-phosphorus codoped carbon dots. *ACS Appl Nano Mater.* 4, 9303–9312 (2021). [https://doi.org/10.1021/ACSANM.1C01810/SUPPL\\_FILE/AN1C01810\\_SI\\_001.PDF](https://doi.org/10.1021/ACSANM.1C01810/SUPPL_FILE/AN1C01810_SI_001.PDF)
20. Kumar, A., Raorane, C.J., Syed, A., Bahkali, A.H., Elgorban, A.M., Raj, V., Kim, S.C.: Synthesis of TiO<sub>2</sub>, TiO<sub>2</sub>/PAni, TiO<sub>2</sub>/PAni/GO nanocomposites and photodegradation of anionic dyes Rose Bengal and thymol blue in visible light. *Environ Res.* 216, 114741 (2023). <https://doi.org/10.1016/J.ENVRES.2022.114741>
21. Bilici, Z., Bouchareb, R., Sacak, T., Yatmaz, H.C., Dizge, N.: Recycling of TiO<sub>2</sub>-containing waste and utilization by photocatalytic degradation of a reactive dye solution. *Water Science and Technology.* 83, 1242–1249 (2021). <https://doi.org/10.2166/WST.2020.606>

22. Zhong, J.L., Yang, L., Lü, F., Xiao, H., Xu, R., Wang, L., Zhu, F., Zhang, Y.: UVA, UVB and UVC induce differential response signaling pathways converged on the eIF2 $\alpha$  phosphorylation. *Photochem Photobiol.* 87, 1092–1104 (2011). <https://doi.org/10.1111/J.1751-1097.2011.00963.X>
23. Wang, C., Li, Y., Wan, J., Hu, Y., Huang, Y., Qiu, J.: Degradation of reactive red (B-3BF) dye wastewater using UV irradiation (254/185 nm) with sodium persulfate in a pilot UV device. *Sci Rep.* 14, (2024). <https://doi.org/10.1038/s41598-024-62967-3>
24. Ayodhya, D., Venkatesham, M., Santoshi kumari, A., Reddy, G.B., Ramakrishna, D., Veerabhadram, G.: Photocatalytic degradation of dye pollutants under solar, visible and UV lights using green synthesised CuS nanoparticles. *J Exp Nanosci.* 11, 418–432 (2016). <https://doi.org/10.1080/17458080.2015.1070312>
25. Safni, M., Audina Putri, R., Vanda Wellia, D., Septiani, U.: Photodegradation of Orange F3R dyes: Effect of light sources and the addition of CN-codoped TiO<sub>2</sub> catalyst. 9, 1–5 (2017)
26. Groeneveld, I., Kanelli, M., Ariese, F., van Bommel, M.R.: Parameters that affect the photodegradation of dyes and pigments in solution and on substrate – An overview. *Dyes and Pigments.* 210, 110999 (2023). <https://doi.org/10.1016/J.DYEPIG.2022.110999>
27. Ollis, D.F.: Solar-assisted photocatalysis for water purification: Issues, data, questions. Presented at the (1991)
28. Ilyas, A., Rafiq, K., Abid, M.Z., Rauf, A., Hussain, E.: Growth of villi-microstructured bismuth vanadate (Vm-BiVO<sub>4</sub>) for photocatalytic degradation of crystal violet dye. *RSC Adv.* 13, 2379–2391 (2023). <https://doi.org/10.1039/D2RA07070G>
29. Zhang, L., Meng, Y., Shen, H., Li, J., Yang, C., Xie, B., Xia, S.: Photocatalytic degradation of rhodamine B by Bi<sub>2</sub>O<sub>3</sub>@LDHs S-scheme heterojunction: Performance, kinetics and mechanism. *Appl Surf Sci.* 567, 150760 (2021). <https://doi.org/10.1016/J.APSUSC.2021.150760>
30. Verma, N., Chundawat, T.S., Chandra, H., Vaya, D.: An efficient time reductive photocatalytic degradation of carcinogenic dyes by TiO<sub>2</sub>-GO nanocomposite. *Mater Res Bull.* 158, 112043 (2023). <https://doi.org/10.1016/J.MATERRESBULL.2022.112043>
31. Bhuiyan, M.S.H., Miah, M.Y., Paul, S.C., Aka, T. Das, Saha, O., Rahaman, M.M., Sharif, M.J.I., Habiba, O., Ashaduzzaman, M.: Green synthesis of iron oxide nanoparticle using Carica papaya leaf extract: application for photocatalytic degradation of remazol yellow RR dye and antibacterial activity. *Heliyon.* 6, e04603 (2020). <https://doi.org/10.1016/J.HELİYON.2020.E04603/ASSET/188546D9-C2E6-4549-ACEC-406E6EA1AEF4/MAIN.ASSETS/GR13.JPG>
32. Ikhlāq, A., Munir, H.M.S., Khan, A., Javed, F., Joya, K.S.: Comparative study of catalytic ozonation and Fenton-like processes using iron-loaded rice husk ash as catalyst for the removal of methylene blue in wastewater. *Ozone Sci Eng.* 41, 250–260 (2019). <https://doi.org/10.1080/01919512.2018.1525276>



33. Ariyanti, D., Maillot, M., Gao, W.: Photo-assisted degradation of dyes in a binary system using TiO<sub>2</sub> under simulated solar radiation. *J Environ Chem Eng.* 6, 539–548 (2018).  
<https://doi.org/10.1016/J.JECE.2017.12.031>
34. Ahmadi, S., Ganjidoust, H.: Using banana peel waste to synthesize BPAC/ZnO nanocomposite for photocatalytic degradation of Acid Blue 25: Influential parameters, mineralization, biodegradability studies. *J Environ Chem Eng.* 9, 106010 (2021).  
<https://doi.org/10.1016/J.JECE.2021.106010>
35. Bagheri, F., Chaibakhsh, N.: Efficient visible-light photocatalytic ozonation for dye degradation using Fe<sub>2</sub>O<sub>3</sub>/MoS<sub>2</sub> nanocomposite. *Sep Sci Technol.* 56, 3022–3032 (2021).  
<https://doi.org/https://doi.org/10.1080/01496395.2020.1861018>
36. Puiatti, G.A., de Carvalho, J.P., de Matos, A.T., Lopes, R.P.: Green synthesis of FeO nanoparticles using Eucalyptus grandis leaf extract: Characterization and application for dye degradation by a (Photo)Fenton-like process. *J Environ Manage.* 311, 114828 (2022).  
<https://doi.org/10.1016/J.JENVMAN.2022.114828>
37. Tsaviv, J.N., Eneji, I.S., Shato'Ato, R., Ahemen, I., Jubu, P.R., Yusof, Y.: Photodegradation, kinetics and non-linear error functions of methylene blue dye using SrZrO<sub>3</sub> perovskite photocatalyst. *Heliyon.* 10, e34517 (2024).  
<https://doi.org/10.1016/J.HELIYON.2024.E34517/ASSET/2562457A-3167-4C63-A5AC-48806BC06D99/MAIN.ASSETS/GR8.JPG>
38. Bhapkar, A., Prasad, R., Jaspal, D., Shirolkar, M., Gheisari, K., Bhambe, S.: Visible light driven photocatalytic degradation of methylene blue by ZnO nanostructures synthesized by glycine nitrate auto combustion route. *Inorg Chem Commun.* 148, (2023).  
<https://doi.org/10.1016/j.inoche.2022.110311>
39. Nguyen Thi Thu, T., Nguyen Thi, N., Tran Quang, V., Nguyen Hong, K., Nguyen Minh, T., Le Thi Hoai, N.: Synthesis, characterisation, and effect of pH on degradation of dyes of copper-doped TiO<sub>2</sub>. *J Exp Nanosci.* 11, 226–238 (2016).  
[https://doi.org/10.1080/17458080.2015.1053541/ASSET/8366A33F-70EF-4A59-B1FC-FACDC66B971E/ASSETS/IMAGES/TJEN\\_A\\_1053541\\_F0006\\_B.GIF](https://doi.org/10.1080/17458080.2015.1053541/ASSET/8366A33F-70EF-4A59-B1FC-FACDC66B971E/ASSETS/IMAGES/TJEN_A_1053541_F0006_B.GIF)
40. Wei, J., Fang, T., Shiraiwa, M.: Effects of acidity on reactive oxygen species formation from secondary organic aerosols. *ACS Environmental Au.* 2, 336–345 (2022).  
<https://doi.org/10.1021/acsenvironau.2c00018>
41. Kazemi, F., Mohamadnia, Z., Kaboudin, B., Karimi, Z.: Photodegradation of methylene blue with a titanium dioxide/polyacrylamide photocatalyst under sunlight. *J Appl Polym Sci.* 133, (2016). <https://doi.org/10.1002/APP.43386>
42. Abbas, R.F., Hassan, M.J.M., Rheima, A.M.: Determination of AY 23 dye using magnetic solid-phase extraction coupled with spectrophotometry: Application of greenness and blueness assessment tools. *Green Analytical Chemistry.* 12, 100179 (2025).  
<https://doi.org/10.1016/J.GREEAC.2024.100179>

43. Yusuff, A.S., Bello, K.A., Azeez, T.M.: Photocatalytic degradation of an anionic dye in aqueous solution by visible light responsive zinc oxide-termite hill composite. *Reaction Kinetics, Mechanisms and Catalysis*. 131, 537–554 (2020). <https://doi.org/10.1007/S11144-020-01839-Z/TABLES/4>
44. Mahdizadeh, H., Nasiri, A., Gharaghani, M.A., Yazdanpanah, G.: Hybrid UV/COP advanced oxidation process using ZnO as a catalyst immobilized on a stone surface for degradation of acid red 18 dye. *MethodsX*. 7, 101118 (2020). <https://doi.org/https://doi.org/10.1016/j.mex.2020.101118>
45. Dadban Shahamat, Y., Masihpour, M., Borghei, P., Hoda Rahmati, S.: Removal of azo red-60 dye by advanced oxidation process O<sub>3</sub>/UV from textile wastewaters using Box-Behnken design. *Inorg Chem Commun*. 143, 109785 (2022). <https://doi.org/https://doi.org/10.1016/j.inoche.2022.109785>
46. Mahdizadeh, H., Dadban Shahamat, Y., Rodríguez-Couto, S.: Discoloration and mineralization of a textile azo dye using a hybrid UV/O<sub>3</sub>/SBR process. *Appl Water Sci*. 11, (2021). <https://doi.org/10.1007/s13201-021-01479-1>
47. Bahadorirad, E., Maghsoudi, S., Jalali, E.: Preparation of nanostructured photocatalyst ZnSnO<sub>3</sub>@S-doped g-C<sub>3</sub>N<sub>4</sub> and its use in DB1 dye degradation through photocatalytic ozonation process. *Heliyon*. 10, (2024). <https://doi.org/10.1016/j.heliyon.2024.e25451>
48. Chakraborty, A., Sarangapany, S., Mishra, U., Mohanty, K.: Green synthesized magnetically separable iron oxide nanoparticles for efficient heterogeneous photo-Fenton degradation of dye Pollutants. *J Clust Sci*. 33, 675–685 (2022). <https://doi.org/10.1007/S10876-021-02010-X>
49. Butt, A.L., Mpinga, J.K., Tichapondwa, S.M.: Photo-fenton oxidation of methyl orange dye using south african ilmenite sands as a catalyst. *Catalysts*. 11, 1452 (2021). <https://doi.org/10.3390/CATAL11121452/S1>
50. Munusamy, T.D., Yee, C.S., Khan, Md.M.R.: Construction of hybrid g-C<sub>3</sub>N<sub>4</sub>/CdO nanocomposite with improved photodegradation activity of RhB dye under visible light irradiation. *Advanced Powder Technology*. 31, 2921–2931 (2020). <https://doi.org/10.1016/j.appt.2020.05.017>
51. Chairungsri, W., Pholchan, P., Sumitsawan, S., Chimupala, Y., Kijjanapanich, P.: Photocatalytic degradation of textile dyeing wastewater using titanium dioxide on a fixed substrate: Optimization of process parameters and continuous reactor tests. *Sustainability* 2023, Vol. 15, Page 12418. 15, 12418 (2023). <https://doi.org/10.3390/SU151612418>
52. Bibi, S., Ahmad, A., Anjum, M.A.R., Haleem, A., Siddiq, M., Shah, S.S., Kahtani, A. Al: Photocatalytic degradation of malachite green and methylene blue over reduced graphene oxide (rGO) based metal oxides (rGO-Fe<sub>3</sub>O<sub>4</sub>/TiO<sub>2</sub>) nanocomposite under UV-visible light irradiation. *J Environ Chem Eng*. 9, 105580 (2021). <https://doi.org/10.1016/J.JECE.2021.105580>

53. Subramani, A.K., Byrappa, K., Ananda, S., Lokanatha Rai, K.M., Ranganathaiah, C., Yoshimura, M.: Photocatalytic degradation of indigo carmine dye using TiO<sub>2</sub> impregnated activated carbon. *Bulletin of Materials Science*. 30, 37–41 (2007).  
<https://doi.org/10.1007/S12034-007-0007-8/METRICS>
54. Ma, C.M., Hong, G.B., Lee, S.C.: Facile synthesis of tin dioxide nanoparticles for photocatalytic degradation of Congo red dye in aqueous solution. *Catalysts* 2020, Vol. 10, Page 792. 10, 792 (2020). <https://doi.org/10.3390/CATAL10070792>
55. Poorsajadi, F., Sayadi, M.H., Hajiani, M., Rezaei, M.R.: Synthesis of CuO/Bi<sub>2</sub>O<sub>3</sub> nanocomposite for efficient and recycling photodegradation of methylene blue dye. *Int J Environ Anal Chem*. 102, 7165–7178 (2022).  
<https://doi.org/10.1080/03067319.2020.1826464>
56. Venkatesh, D., Pavalamalar, S., Anbalagan, K.: Selective photodegradation on dual dye system by recoverable nano SnO<sub>2</sub> photocatalyst. *J Inorg Organomet Polym Mater*. 29, 939–953 (2019). <https://doi.org/10.1007/s10904-018-01069-w>
57. Raashid, M., Kazmi, M., Ikhlaq, A., Sulaiman, M., Akram, A., Afaf, A., Shafaqat, S., Masood, Z., Zafar, A.M., Al-Farraj, S., Sillanpää, M.: Removal of acid red dye 1 from textile wastewater by heterogenous photocatalytic ozonation employing titanium dioxide and iron zeolite. *Discover Chemical Engineering* 2024 4:1. 4, 1–14 (2024).  
<https://doi.org/10.1007/S43938-024-00059-4>
58. Bousalah, D., Zazoua, H., Boudjemaa, A., Benmounah, A., Bachari, khaldoun: Degradation of Indigotine food dye by Fenton and photo-Fenton processes. *Int J Environ Anal Chem*. 102, 4609–4622 (2022). <https://doi.org/10.1080/03067319.2020.1786546>
59. Dai, N., Yi, S., Zhang, X., Feng, L., Ding, H., Song, D., Liu, X., Rao, J., Zhang, Y.: Typical synthesis of an iron-modified Laponite @diatomite composite for photo-Fenton degradation of methyl orange dyes. *Appl Surf Sci*. 607, 154886 (2023).  
<https://doi.org/10.1016/J.APSUSC.2022.154886>
60. Elsayed, E.M., Elnouby, M.S., Gouda, S.M.H., Elessawy, N.A., Santos, D.M.F.: Effect of the morphology of tungsten oxide embedded in sodium alginate/polyvinylpyrrolidone composite beads on the photocatalytic degradation of methylene blue dye solution. *Materials* 2020, Vol. 13, Page 1905. 13, 1905 (2020). <https://doi.org/10.3390/MA13081905>
61. Sharifian, K., Mahdikhah, V., Sheibani, S.: Ternary Ag@SrTiO<sub>3</sub>@CNT plasmonic nanocomposites for the efficient photodegradation of organic dyes under the visible light irradiation. *Ceram Int*. 47, 22741–22752 (2021).  
<https://doi.org/10.1016/J.CERAMINT.2021.04.291>
62. Murugesan, A., Loganathan, M., Senthil Kumar, P., Vo, D.V.N.: Cobalt and nickel oxides supported activated carbon as an effective photocatalysts for the degradation methylene blue dye from aquatic environment. *Sustain Chem Pharm*. 21, 100406 (2021).  
<https://doi.org/10.1016/J.SCP.2021.100406>

63. Siddique, M., Khan, N.M., Saeed, M.: Photocatalytic activity of bismuth ferrite nanoparticles synthesized via sol-gel route. *Zeitschrift für Physikalische Chemie*. 233, 595–607 (2019). <https://doi.org/10.1515/ZPCH-2018-1225/MACHINEREADABLECITATION/RIS>
64. Luo, Y., Zheng, A., Li, J., Han, Y., Xue, M., Zhang, L., Yin, Z., Xie, C., Chen, Z., Ji, L., Hong, Z., Xie, X.: Integrated adsorption and photodegradation of tetracycline by bismuth oxycarbonate/biochar nanocomposites. *Chemical Engineering Journal*. 457, 141228 (2023). <https://doi.org/10.1016/J.CEJ.2022.141228>
65. Moslehnejad, N., Jahangiri, M., Vafaei, F., Salavati-Niasari, M.: Synthesis and characterization of ZnO–Ce nanophotocatalyst and their application for the removal of dye (Reactive red 198) by degradation process: Kinetics, thermodynamics and experimental design. *Int J Hydrogen Energy*. 47, 23980–23993 (2022). <https://doi.org/10.1016/J.IJHYDENE.2022.05.189>
66. Osman, H., Su, Z., Ma, X.: Efficient photocatalytic degradation of Rhodamine B dye using ZnO/graphitic C3N4 nanocomposites synthesized by microwave. *Environ Chem Lett*. 15, 435–441 (2017). <https://doi.org/10.1007/S10311-017-0604-8/FIGURES/4>
67. Velidandi, A., Pabbathi, N.P.P., Baadhe, R.R.: Study of parameters affecting the degradation of rhodamine-B and methyl orange dyes by *Annona muricata* leaf extract synthesized nanoparticles as well as their recyclability. *J Mol Struct*. 1236, (2021). <https://doi.org/10.1016/j.molstruc.2021.130287>
68. Usman, M., Ahmed, A., Khalid, A., Rafiq, M., Algarni, M., Albalawi, A.N., Aldhafeeri, Z.M., Hasan, M.: Unveiling the synthesis of magnetically separable magnetite nanoparticles anchored over reduced graphene oxide for enhanced visible-light-driven photocatalytic degradation of dyes. *Diam Relat Mater*. 149, 111575 (2024). <https://doi.org/10.1016/j.diamond.2024.111575>
69. Nisar, A., Saeed, M., Muneer, M., Usman, M., Khan, I.: Synthesis and characterization of ZnO decorated reduced graphene oxide (ZnO-rGO) and evaluation of its photocatalytic activity toward photodegradation of methylene blue. *Environmental Science and Pollution Research*. 29, 418–430 (2022). <https://doi.org/10.1007/S11356-021-13520-6>
70. Barakat, N.A.M., Kanjwal, M.A., Chronakis, I.S., Kim, H.Y.: Influence of temperature on the photodegradation process using Ag-doped TiO<sub>2</sub> nanostructures: Negative impact with the nanofibers. *J Mol Catal A Chem*. 366, 333–340 (2013). <https://doi.org/10.1016/J.MOLCATA.2012.10.012>
71. Ouni, S., Yahia, F., BelHaj Mohamed, N., Bouzidi, M., S. Alshammari, A., Abdulaziz, F., Bonilla-Petriciolet, A., Mohamed, M., R. Khan, Z., Chaaben, N., Haouari, M.: Effective removal of textile dye via synergy of adsorption and photocatalysis over ZnS nanoparticles: Synthesis, modeling, and mechanism. *Heliyon*. 10, e36949 (2024). <https://doi.org/10.1016/J.HELİYON.2024.E36949/ASSET/3713C446-29A1-42AA-8657-C6A51117E9E6/MAIN.ASSETS/GR4.JPG>

72. Shams, M., Guiney, L.M., Ramesh, M., Hersam, M.C., Chowdhury, I.: Effects of sunlight on the fate of graphene oxide and reduced graphene oxide nanomaterials in the natural surface water. *Science of The Total Environment*. 874, 162427 (2023).  
<https://doi.org/10.1016/J.SCITOTENV.2023.162427>
73. Garg, N., Bera, S., Rastogi, L., Ballal, A., Balaramakrishna, M. V.: Synthesis and characterization of L-asparagine stabilised gold nanoparticles: Catalyst for degradation of organic dyes. *Spectrochim Acta A Mol Biomol Spectrosc*. 232, 118126 (2020).  
<https://doi.org/10.1016/J.SAA.2020.118126>
74. Saldanha, L.A.S., Santos, N.T. das G., Tomaz, E.: Photocatalytic ethylbenzene degradation associated with ozone (TiO<sub>2</sub>/UV/O<sub>3</sub>) under different percentages of catalytic coating area: Evaluation of process parameters. *Sep Purif Technol*. 263, 118344 (2021).  
<https://doi.org/10.1016/J.SEPPUR.2021.118344>
75. Abdelbaky, M., Abdelghany, A.M., Oraby, A.H., Abdelrazek, E.M., Rashad, M.M.: Efficacious elimination of crystal violet pollutant via photo-Fenton process based on Gd(2-x)La(x)Zr<sub>2</sub>O<sub>7</sub> nanoparticles. *Sci Rep*. 13, 7723 (2023).  
<https://doi.org/10.1038/s41598-023-34838-w>
76. Abramovic, B., Despotovic, V., Šojic, D., Fincur, N.: Mechanism of clomazone photocatalytic degradation: Hydroxyl radical, electron and hole scavengers. *Reaction Kinetics, Mechanisms and Catalysis*. 115, 67–79 (2015). <https://doi.org/10.1007/S11144-014-0814-Z>
77. Khan, S., Noor, T., Iqbal, N., Yaqoob, L.: Photocatalytic dye degradation from textile wastewater: A review. *ACS Omega*. 9, 21751–21767 (2024).  
[https://doi.org/10.1021/ACSSOMEGA.4C00887/ASSET/IMAGES/LARGE/AO4C00887\\_0007.JPEG](https://doi.org/10.1021/ACSSOMEGA.4C00887/ASSET/IMAGES/LARGE/AO4C00887_0007.JPEG)
78. Nzaba, S.K.M., Mmelesi, O.K., Malefane, M.E., Mafa, P.J., Mamba, B.B., Kuvarega, A.T.: Comparative study of visible-light active BiOI and N,Pd-TiO<sub>2</sub> photocatalysts: Catalytic ozonation for dye degradation. *Colloids Surf A Physicochem Eng Asp*. 684, 133167 (2024).  
<https://doi.org/10.1016/J.COLSURFA.2024.133167>
79. Habib, I.Y., Burhan, J., Jaladi, F., Lim, C.M., Usman, A., Kumara, N.T.R.N., Tsang, S.C.E., Mahadi, A.H.: Effect of Cr doping in CeO<sub>2</sub> nanostructures on photocatalysis and H<sub>2</sub>O<sub>2</sub> assisted methylene blue dye degradation. *Catal Today*. 375, 506–513 (2021).  
<https://doi.org/10.1016/J.CATTOD.2020.04.008>
80. Mahmoodi, N.M.: Photocatalytic degradation of textile dyes using ozonation and magnetic nickel ferrite nanoparticle. *Progress in Color, Colorants and Coatings*. 9, 163–171 (2016).  
<https://doi.org/10.30509/PCCC.2016.75883>
81. Pandian, L., Rajasekaran, R., Govindan, P.: Nanophotocatalytic ozonation of textile dyeing wastewater using Cu-Zno nanocatalyst and study of reactor influencing parameters. *Oriental Journal of Chemistry*. 35, 384–390 (2019). <https://doi.org/10.13005/ojc/350148>

82. Rajeswari, R., Poongodi, G.: Study on degradation of textile dyes by photocatalytic ozonation assisted with tin doped zinc oxide nanorods. *International Journal of Nanoscience and Nanotechnology*. 20, 63–76 (2024). <https://doi.org/10.22034/ijnn.2024.531286.2050>
83. Chen, P., Cheng, Z., Zhang, X., Zhang, L., Zhang, X., Tang, J., Qiu, F.: Efficient degradation of dye wastewater by catalytic ozonation reactive ceramic membrane with facile spraying of nano TiMn oxides: A pilot scale attempt. *Journal of Water Process Engineering*. 55, 104143 (2023). <https://doi.org/10.1016/J.JWPE.2023.104143>
84. Shen, Y., Xu, Q., Wei, R., Ma, J., Wang, Y.: Mechanism and dynamic study of reactive red X-3B dye degradation by ultrasonic-assisted ozone oxidation process. *Ultrason Sonochem*. 38, 681–692 (2017). <https://doi.org/10.1016/J.ULTSONCH.2016.08.006>
85. Rahmati, R., Nayebi, B., Ayati, B.: Investigating the effect of hydrogen peroxide as an electron acceptor in increasing the capability of slurry photocatalytic process in dye removal. *Water Science and Technology*. 83, 2414–2423 (2021). <https://doi.org/10.2166/WST.2021.136>
86. Setyaningtyas, T., Riyani, K., Handayani, S.N., Firdharini, C.: Degradation of Congo red in batik wastewater using Fenton reagent under visible rays. *IOP Conf Ser Mater Sci Eng*. 509, (2019). <https://doi.org/10.1088/1757-899X/509/1/012027>
87. Khalaf, H.A.F., El-Baki, R.F.A.: Effectiveness of ceria and stania nanoparticles in photodegradation Tenoxicam antibiotics using UV-H<sub>2</sub>O<sub>2</sub>. *Iranian Journal of Catalysis*. 13, 285–297 (2023). <https://doi.org/10.30495/IJC.2023.1985433.2006>
88. Cao, V.D., Nong, L.X., Nguyen, V.H., Tran, T. V., Vu, H.T., Nguyen, C. V., Do, S.T.: High degradation of BIVO<sub>4</sub> nanoparticle for organic dyes under visible light irradiation mediated by S<sub>2</sub>O<sub>8</sub>. *IOP Conf Ser Mater Sci Eng*. 736, 042019 (2020). <https://doi.org/10.1088/1757-899X/736/4/042019>
89. Monteagudo, J.M., Durán, A., Martín, I.S., Vellón, B.: Photocatalytic degradation of aniline by solar/TiO<sub>2</sub> system in the presence of the electron acceptors Na<sub>2</sub>S<sub>2</sub>O<sub>8</sub> and H<sub>2</sub>O<sub>2</sub>. *Sep Purif Technol*. 238, 116456 (2020). <https://doi.org/10.1016/J.SEPPUR.2019.116456>
90. Paul, S.C., Bhowmik, S., Nath, M.R., Islam, Md.S., Kanti Paul, S., Neazi, J., Monir, T.S.B., Dewanjee, S., Abdus Salam, M.: Silver Nanoparticles Synthesis in a Green Approach: Size Dependent Catalytic Degradation of Cationic and Anionic Dyes. *Oriental Journal of Chemistry*. 36, 353–360 (2020). <https://doi.org/10.13005/OJC/360301>
91. Barzinjy, A.A., Hamad, S.M., Aydın, S., Mukhtar, ·, Ahmed, H., Faiq, ·, Hussain, H.S.: Green and eco-friendly synthesis of Nickel oxide nanoparticles and its photocatalytic activity for methyl orange degradation. *Journal of Materials Science: Materials in Electronics*. 31, 11303–11316 (2020). <https://doi.org/10.1007/s10854-020-03679-y>
92. Şahin, Ö., Baytar, O., Kutluay, S., Ekinci, A.: Potential of nickel oxide catalyst from banana peel extract via green synthesis method in both photocatalytic reduction of methylene blue

- and generation of hydrogen from sodium borohydride hydrolysis. *J Photochem Photobiol A Chem.* 448, 115301 (2024). <https://doi.org/10.1016/J.PHOTOCHEM.2023.115301>
93. Gola, D., kriti, A., Bhatt, N., Bajpai, M., Singh, A., Arya, A., Chauhan, N., Srivastava, S.K., Tyagi, P.K., Agrawal, Y.: Silver nanoparticles for enhanced dye degradation. *Current Research in Green and Sustainable Chemistry.* 4, 100132 (2021). <https://doi.org/10.1016/J.CRGSC.2021.100132>
94. Kanchana, S., Vijayalakshmi, R.: Photocatalytic degradation of organic dyes by PEG and PVP capped Cu, Ni and Ag nanoparticles in the presence of NaBH<sub>4</sub> in aqueous medium. *Journal of Water and Environmental Nanotechnology.* 5, 294–306 (2020). <https://doi.org/10.22090/JWENT.2020.04.001>
95. Al Rubai, H.F., Sultan, M.S., Abed, G.M.: Enhancing the removal efficiency of azo de using sodium borohydride in the presence of inorganic nano catalysts. *Green Analytical Chemistry.* 100194 (2024). <https://doi.org/10.1016/J.GREEAC.2024.100194>
96. Al-Shehri, A.S., Zaheer, Z., Alsudairi, A.M., Kosa, S.A.: Photo-oxidative decolorization of Brilliant Blue with AgNPs as an activator in the presence of K<sub>2</sub>S<sub>2</sub>O<sub>8</sub> and NaBH<sub>4</sub>. *ACS Omega.* 6, 27510–27526 (2021). [https://doi.org/10.1021/ACSOMEGA.1C04501/ASSET/IMAGES/MEDIUM/AO1C04501\\_M024.GIF](https://doi.org/10.1021/ACSOMEGA.1C04501/ASSET/IMAGES/MEDIUM/AO1C04501_M024.GIF)
97. Shabil Sha, M., Anwar, H., Musthafa, F.N., Al-Lohedan, H., Alfarwati, S., Rajabathar, J.R., Khalid Alahmad, J., Cabibihan, J.J., Karnan, M., Kumar Sadasivuni, K.: Photocatalytic degradation of organic dyes using reduced graphene oxide (rGO). *Scientific Reports* 2024 14:1. 14, 1–14 (2024). <https://doi.org/10.1038/s41598-024-53626-8>
98. Nosaka, Y., Nosaka, A.Y.: Generation and detection of reactive oxygen species in photocatalysis. *Chem Rev.* 117, 11302–11336 (2017). [https://doi.org/10.1021/ACS.CHEMREV.7B00161/ASSET/IMAGES/MEDIUM/CR-2017-00161A\\_0001.GIF](https://doi.org/10.1021/ACS.CHEMREV.7B00161/ASSET/IMAGES/MEDIUM/CR-2017-00161A_0001.GIF)
99. He, Y., Li, H., Xiao, X., Zhao, X.: Polymer degradation: Category, mechanism and development prospect. *E3S Web of Conferences.* 290, 01012 (2021). <https://doi.org/10.1051/E3SCONF/202129001012>
100. Mak, C.H., Han, X., Du, M., Kai, J.-J., Tsang, K.F., Jia, G., Cheng, K.-C., Shen, H.-H., Hsu, H.-Y.: Heterogenization of homogeneous photocatalysts utilizing synthetic and natural support materials. *J Mater Chem A Mater.* 9, 4454–4504 (2021). <https://doi.org/10.1039/D0TA08334H>
101. Zou, L., Zhu, B.: The synergistic effect of ozonation and photocatalysis on color removal from reused water. *J Photochem Photobiol A Chem.* 196, 24–32 (2008). <https://doi.org/10.1016/j.jphotochem.2007.11.008>

102. G., N., A., D.R., A., A.I., R.L., J.: Tuning the optical band gap of pure TiO<sub>2</sub> via photon induced method. *Optik (Stuttg)*. 179, 889–894 (2019).  
<https://doi.org/10.1016/J.IJLEO.2018.11.009>
103. Jafarova, V.N., Orudzhev, G.S.: Structural and electronic properties of ZnO: A first-principles density-functional theory study within LDA(GGA) and LDA(GGA)+U methods. *Solid State Commun*. 325, 114166 (2021). <https://doi.org/10.1016/J.SSC.2020.114166>
104. Mubeen, A., Majid, A., Alkhedher, M., Tag-ElDin, E.M., Bulut, N.: Structural and electronic properties of SnO downscaled to monolayer. *Materials*. 15, 5578 (2022).  
<https://doi.org/10.3390/ma15165578>
105. Oudah, M.H., Hasan, M.H., Abd, A.N.: Synthesis of copper oxide thin films by electrolysis method based on Porous Silicon for Solar Cell Applications. *IOP Conf Ser Mater Sci Eng*. 757, 012051 (2020). <https://doi.org/10.1088/1757-899X/757/1/012051>
106. Amjad, M., Mohyuddin, A., Ulfat, W., Goh, H.H., Dzarfan Othman, M.H., Kurniawan, T.A.: UV-blocking and photocatalytic properties of Ag-coated cotton fabrics with Si binders for photo-degradation of recalcitrant dyes in aqueous solutions under sunlight. *J Environ Manage*. 353, (2024). <https://doi.org/10.1016/j.jenvman.2024.120287>
107. Gabet, A., Guy, C., Fazli, A., Métivier, H., de Brauer, C., Brigante, M., Mailhot, G.: The ability of recycled magnetite nanoparticles to degrade carbamazepine in water through photo-Fenton oxidation at neutral pH. *Sep Purif Technol*. 317, 123877 (2023).  
<https://doi.org/10.1016/J.SEPPUR.2023.123877>
108. Gou, Y., Peng, L., Xu, H., Li, S., Liu, C., Wu, X., Song, S., Yang, C., Song, K., Xu, Y.: Insights into the degradation mechanisms and pathways of cephalexin during homogeneous and heterogeneous photo-Fenton processes. *Chemosphere*. 285, 131417 (2021).  
<https://doi.org/10.1016/j.chemosphere.2021.131417>
109. Youcai, Z.: Leachate treatment engineering processes. *Pollution Control Technology for Leachate from Municipal Solid Waste*. 361–522 (2018).  
<https://doi.org/https://doi.org/10.1016/B978-0-12-815813-5.00005-X>
110. Samarghandi, M.R., Dargahi, A., Zolghadr Nasab, H., Ghahramani, E., Salehi, S.: Degradation of azo dye Acid Red 14 (AR14) from aqueous solution using H<sub>2</sub>O<sub>2</sub>/nZVI and S<sub>2</sub>O<sub>8</sub><sup>2-</sup>/nZVI processes in the presence of UV irradiation. *Water Environ Res*. 92, 1173–1183 (2020). <https://doi.org/10.1002/WER.1312>
111. Wang, X., Zhang, L.: Kinetic study of hydroxyl radical formation in a continuous hydroxyl generation system. *RSC Adv*. 8, 40632–40638 (2018). <https://doi.org/10.1039/C8RA08511K>
112. Sitta, E., Gómez-Marín, A.M., Aldaz, A., Feliu, J.M.: Electrocatalysis of H<sub>2</sub>O<sub>2</sub> reduction/oxidation at model platinum surfaces. *Electrochem commun*. 33, 39–42 (2013).  
<https://doi.org/10.1016/J.ELECOM.2013.04.014>



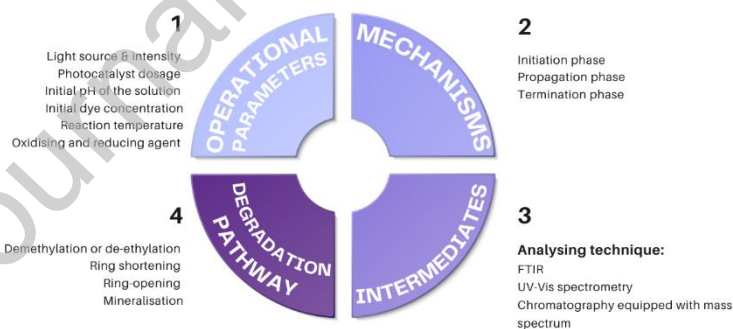
113. Chen, X., Xue, Z., Yao, Y., Wang, W., Zhu, F., Hong, C.: Oxidation degradation of rhodamine B in aqueous by UV/S<sub>2</sub>O<sub>8</sub><sup>2-</sup> treatment system. *International Journal of Photoenergy*. 2012, (2012). <https://doi.org/10.1155/2012/754691>
114. Saha, D., Desipio, M.M., Hoinkis, T.J., Smeltz, E.J., Thorpe, R., Hensley, D.K., Fischer-Drowos, S.G., Chen, J.: Influence of hydrogen peroxide in enhancing photocatalytic activity of carbon nitride under visible light: An insight into reaction intermediates. *J Environ Chem Eng*. 6, 4927–4936 (2018). <https://doi.org/10.1016/J.JECE.2018.07.030>
115. Gupta, N., Singh, H.P., Sharma, R.K.: Metal nanoparticles with high catalytic activity in degradation of methyl orange: An electron relay effect. *J Mol Catal A Chem*. 335, 248–252 (2011). <https://doi.org/10.1016/J.MOLCATA.2010.12.001>
116. Ammar, S.H., Khadim, H.J., Al-Farraji, A.: Synthesis of Ni@ $\gamma$ -Al<sub>2</sub>O<sub>3</sub>@PDA/SiW recyclable nanocatalyst and its catalytic reduction and antibacterial activities. *Nanotechnology for Environmental Engineering*. 5, 16 (2020). <https://doi.org/10.1007/s41204-020-00082-0>
117. Zainal Abidin, A., Abu Bakar, N.H.H., Ng, E.P., Tan, W.L.: Rapid degradation of methyl orange by Ag doped Zeolite X in the presence of borohydride. *Journal of Taibah University for Science*. 11, 1070–1079 (2017). <https://doi.org/10.1016/J.JTUSCI.2017.06.004>
118. Benkhaya, S., M'rabet, S., El Harfi, A.: Classifications, properties, recent synthesis and applications of azo dyes. *Heliyon*. 6, e03271 (2020). <https://doi.org/10.1016/J.HELIYON.2020.E03271>
119. Mahapatra, N.N.: *Textile dyes*. WPI Publishing (2016)
120. Bopape, D.A., Ntsendwana, B., Mabasa, F.D.: Photocatalysis as a pre-discharge treatment to improve the effect of textile dyes on human health: A critical review. *Heliyon*. 10, e39316 (2024). <https://doi.org/10.1016/J.HELIYON.2024.E39316>
121. Ovchinnikov, O. V., Evtukhova, A. V., Kondratenko, T.S., Smirnov, M.S., Khokhlov, V.Y., Erina, O. V.: Manifestation of intermolecular interactions in FTIR spectra of methylene blue molecules. *Vib Spectrosc*. 86, 181–189 (2016). <https://doi.org/10.1016/J.VIBSPEC.2016.06.016>
122. Majeed, A., Ibrahim, A.H., Al-Rawi, S.S., Iqbal, M.A., Kashif, M., Yousif, M., Abidin, Z.U., Ali, S., Arbaz, M., Hussain, S.A.: Green organo-photooxidative method for the degradation of methylene blue dye. *ACS Omega*. 9, 12069–12083 (2024). <https://doi.org/10.1021/acsomega.3c09989>
123. Mohamadi, S., Ghorbanali, M.: Adsorption and UV-assisted photodegradation of methylene blue by CeO<sub>2</sub>-decorated graphene sponge. *Sep Sci Technol*. 56, 507–517 (2021). <https://doi.org/10.1080/01496395.2020.1728325>
124. Alvarado, J.A., Gonzalez, G.S.A., Cao, G.: Rapid and efficient mineralization of methylene blue dye (above 95 % in 20 min) catalyzed by ZnO nanoparticles under sunlight. *Materials Today Sustainability*. 27, 100883 (2024). <https://doi.org/10.1016/J.MTSUST.2024.100883>

125. Vithalani, P., Bhatt, N.: A review on toxicology study and approach of xanthene dyes. (2023)
126. Ajiboye, T.O., Oyewo, O.A., Onwudiwe, D.C.: Adsorption and photocatalytic removal of Rhodamine B from wastewater using carbon-based materials. *FlatChem*. 29, 100277 (2021). <https://doi.org/10.1016/J.FLATC.2021.100277>
127. Ma, D., Tang, J., He, G., Xue, Y., Pan, S., Liu, F., Zhao, J.: Enhancing photocatalytic degradation of rhodamine B with visible-light-driven HCl-assisted Bi<sub>2</sub>O<sub>3</sub> photocatalysts: Activity, mechanism, and pathways. *Mater Sci Semicond Process*. 181, 108672 (2024). <https://doi.org/10.1016/J.MSSP.2024.108672>
128. Zhu, J.L., Chen, S.P., Lin, W., Huang, H.D., Li, Z.M.: Cellulose mineralization with in-situ synthesized amorphous titanium dioxide for enhanced adsorption and auto-accelerating photocatalysis on water pollutant. *Chemical Engineering Journal*. 456, 141036 (2023). <https://doi.org/10.1016/J.CEJ.2022.141036>
129. Ma, D., Tang, J., He, G., Pan, S.: Investigation of the photocatalytic performance, mechanism, and degradation pathways of rhodamine B with Bi<sub>2</sub>O<sub>3</sub> microrods under visible-light irradiation. *Materials*. 17, 957 (2024). <https://doi.org/10.3390/MA17040957/S1>
130. Rao, Z., Lu, G., Chen, L., Mahmood, A., Shi, G., Tang, Z., Xie, X., Sun, J.: Photocatalytic oxidation mechanism of Gas-Phase VOCs: Unveiling the role of holes, •OH and •O<sub>2</sub><sup>-</sup>. *Chemical Engineering Journal*. 430, 132766 (2022). <https://doi.org/10.1016/J.CEJ.2021.132766>
131. Chen, Y., Ma, D., He, G., Pan, S.: Effects of pH on the photocatalytic activity and degradation mechanism of rhodamine B over fusiform Bi photocatalysts under visible light. *Water (Switzerland)*. 16, 2389 (2024). <https://doi.org/10.3390/W16172389/S1>
132. Chiu, Y.-H., Chang, T.-F., Chen, C.-Y., Sone, M., Hsu, Y.-J.: Mechanistic insights into photodegradation of organic dyes using heterostructure photocatalysts. *Catalysts*. 9, 430 (2019). <https://doi.org/10.3390/catal9050430>
133. Mishra, P.K., Dobhal, R., Rini, E.G., Kumar, M., Sen, S.: Rapid organic dye degradation and wavelength dependent sensing study in Cu<sub>1-x</sub>Fe<sub>x</sub>O. *Ceram Int*. 48, 5995–6006 (2022). <https://doi.org/https://doi.org/10.1016/j.ceramint.2021.11.135>
134. Dinh, V.P., Huynh, T.D.T., Le, H.M., Nguyen, V.D., Dao, V.A., Hung, N.Q., Tuyen, L.A., Lee, S., Yi, J., Nguyen, T.D., Tan, L. V.: Insight into the adsorption mechanisms of methylene blue and chromium(III) from aqueous solution onto pomelo fruit peel. *RSC Adv*. 9, 25847–25860 (2019). <https://doi.org/10.1039/c9ra04296b>
135. Liu, J., Zhang, T., Wang, Z., Dawson, G., Chen, W.: Simple pyrolysis of urea into graphitic carbon nitride with recyclable adsorption and photocatalytic activity. *J Mater Chem*. 21, 14398 (2011). <https://doi.org/10.1039/c1jm12620b>
136. Nair, R.G., Mazumdar, S., Modak, B., Bapat, R., Ayyub, P., Bhattacharyya, K.: The role of surface O-vacancies in the photocatalytic oxidation of methylene blue by Zn-doped TiO<sub>2</sub>: A

- Mechanistic approach. *J Photochem Photobiol A Chem.* 345, 36–53 (2017).  
<https://doi.org/10.1016/J.JPHOTOCHEM.2017.05.016>
137. Phuruangrat, A., Thungprasert, S., Sakhon, T., Kuntalue, B., Thongtem, T., Thongtem, S.: Degradation of rhodamine B photocatalyzed by Eu-doped CdS nanowires illuminated by visible radiation. *Journal of the Indian Chemical Society.* 99, 100349 (2022).  
<https://doi.org/10.1016/J.JICS.2022.100349>
138. Hu, L., Deng, G., Lu, W., Pang, S., Hu, X.: Deposition of CdS nanoparticles on MIL-53(Fe) metal-organic framework with enhanced photocatalytic degradation of RhB under visible light irradiation. *Appl Surf Sci.* 410, 401–413 (2017).  
<https://doi.org/10.1016/J.APSUSC.2017.03.140>
139. Fu, H., Pan, C., Yao, W., Zhu, Y.: Visible-light-induced degradation of rhodamine B by nanosized Bi<sub>2</sub>WO<sub>6</sub>. *Journal of Physical Chemistry B.* 109, 22432–22439 (2005).  
[https://doi.org/10.1021/JP052995J/SUPPL\\_FILE/JP052995J\\_S.PDF](https://doi.org/10.1021/JP052995J/SUPPL_FILE/JP052995J_S.PDF)
140. Chen, J., Yang, M., Zhang, H., Chen, Y., Ji, Y., Yu, R., Liu, Z.: Boosting the activation of molecular oxygen and the degradation of rhodamine B in polar-functional-group-modified g-C<sub>3</sub>N<sub>4</sub>. *Molecules.* 29, 3836 (2024). <https://doi.org/10.3390/MOLECULES29163836/S1>
141. Zeng, Z., Li, K., Yuan, T., Liang, Y., Yang, J., Yang, G., Wang, K., Xiong, Z.: Facile synthesis of BiOCl/g-C<sub>3</sub>N<sub>4</sub> heterojunction via in situ hydrolysis of Bi nanospheres: a high-efficiency visible-light-driven photocatalyst. *Journal of Materials Science: Materials in Electronics.* 32, 9972–9989 (2021). <https://doi.org/10.1007/S10854-021-05655-6/FIGURES/14>
142. Martin, N., Leprince-Wang, Y.: HPLC-MS and UV–visible coupled analysis of methylene blue photodegradation by hydrothermally grown ZnO Nanowires. *physica status solidi (a).* 218, 2100532 (2021). <https://doi.org/10.1002/PSSA.202100532>
143. Shi, W., Fang, W.-X., Wang, J.-C., Qiao, X., Wang, B., Guo, X.: pH-controlled mechanism of photocatalytic RhB degradation over g-C<sub>3</sub>N<sub>4</sub> under sunlight irradiation. *Photochemical & Photobiological Sciences.* 20, 303–313 (2021). <https://doi.org/10.1007/s43630-021-00019-9>
144. Wang, T., Zheng, J., Cai, J., Liu, Q., Zhang, X.: Visible-light-driven photocatalytic degradation of dye and antibiotics by activated biochar composited with K<sup>+</sup> doped g-C<sub>3</sub>N<sub>4</sub>: Effects, mechanisms, actual wastewater treatment and disinfection. *Science of The Total Environment.* 839, 155955 (2022). <https://doi.org/10.1016/j.scitotenv.2022.155955>
145. Yang, J., Zhu, H., Peng, Y., Li, P., Chen, S., Yang, B., Zhang, J.: Photocatalytic performance and degradation pathway of Rhodamine B with TS-1/C<sub>3</sub>N<sub>4</sub> composite under visible light. *Nanomaterials.* 10, 756 (2020). <https://doi.org/10.3390/nano10040756>
146. Khanam, S., Rout, S.K.: Improved photocatalytic activity of hydrothermally prepared Bi<sub>2</sub>WO<sub>6</sub> in degradation of Rhodamine B and methylene blue. *Indian Journal of Pure & Applied Physics.* 60, 1–10 (2022). <https://doi.org/10.56042/ijpap.v60i7.61436>

147. Wu, C.H.: Effects of sonication on decolorization of C.I. Reactive Red 198 in UV/ZnO system. *J Hazard Mater.* 153, 1254–1261 (2008).  
<https://doi.org/10.1016/J.JHAZMAT.2007.09.086>
148. Zubrik, A., Jáger, D., Mačingová, E., Matik, M., Hredzák, S.: Spontaneous degradation of methylene blue adsorbed on magnetic biochars. *Scientific Reports* 2023 13:1. 13, 1–10 (2023). <https://doi.org/10.1038/s41598-023-39976-9>
149. Yashni, G., Al-Gheethi, A., Mohamed, R., Arifin, S.N.H., Salleh, S.N.A.M.: Photodegradation of basic red 51 in hair dye greywater by zinc oxide nanoparticles using central composite design. *Reaction Kinetics, Mechanisms and Catalysis.* 130, 567–588 (2020). <https://doi.org/10.1007/S11144-020-01792-X/FIGURES/6>
150. Ahmed, T., Noman, M., Shahid, M., Niazi, M.B.K., Hussain, S., Manzoor, N., Wang, X., Li, B.: Green synthesis of silver nanoparticles transformed synthetic textile dye into less toxic intermediate molecules through LC-MS analysis and treated the actual wastewater. *Environ Res.* 191, 110142 (2020). <https://doi.org/10.1016/j.envres.2020.110142>

## Graphical abstract



## Declaration of interests

The authors declare that they have no known competing financial interests or personal relationships that could have appeared to influence the work reported in this paper.

The authors declare the following financial interests/personal relationships which may be considered as potential competing interests:

Journal Pre-proof